STREST

D 4.3

DELIVERABLE

PROJECT INFORMATION

Project Title:	**Harmonized approach to stress tests for critical infrastructures against natural hazards**
Acronym:	**STREST**
Project N°:	603389
Call N°:	FP7-ENV-2013-two-stage
Project start:	01 October 2013
Duration:	36 months

DELIVERABLE INFORMATION

Deliverable Title:	**Guidelines for performance and consequences assessment of multiple-site, low-risk, high-impact, non-nuclear critical infrastructures (exposed to multiple natural hazards, etc.)**
Date of issue:	30 September 2015
Work Package:	WP4 – Vulnerability models for the performance and consequences assessment in stress tests of CIs
Editor/Author:	Helen Crowley (EUCENTRE)
Reviewer:	Georgios Tsionis (JRC)

REVISION: Version 1

SEVENTH FRAMEWORK PROGRAMME

Project Coordinator:	Prof. Domenico Giardini
Institution:	ETH Zürich
e-mail:	giardini@sed.ethz.ch
fax:	+ 41 446331065
telephone:	+ 41 446332610

Abstract

These guidelines provide a framework for the performance and consequences assessment of multiple-site, low-risk high-impact non-nuclear critical infrastructures subjected to strong ground shaking during earthquakes. Industrial districts have been selected as an example of this type of non-nuclear critical infrastructure for the purposes of these guidelines. Precast concrete warehouses that are typically found in industrial districts in Europe, and that have demonstrated high levels of damage in past earthquakes (described further in STREST Deliverable 2.3) are used as an application of the guidelines. Damage to these buildings can affect the structural system, the non-structural components (such as the external cladding), and the contents of the building, thus leading to a number of direct economic losses and the time required to repair the damage leads to additional business interruption losses, all of which are covered herein.

Keywords: multi-site risk, industrial district, fragility, structural, non-structural, contents, business interruption

Acknowledgments

The research leading to these results has received funding from the European Community's Seventh Framework Programme [FP7/2007-2013] under grant agreement n° 603389.

Deliverable Contributors

EUCENTRE	Helen Crowley
	Chiara Casotto
University of Ljubljana	Matjaz Dolšek
	Anze Babič

Table of Contents

List of Figures

List of Tables

1 Introduction

1.1 OUTLINE OF THE GUIDELINES

This deliverable provides a framework for the performance and consequences assessment of ***multiple-site, low-rise, high-impact non-nuclear critical infrastructures*** subjected to strong ground shaking during earthquakes. Industrial districts have been selected as an example of this type of non-nuclear critical infrastructure for the purposes of these guidelines. Precast concrete warehouses that are typically found in industrial districts in Europe, and that have demonstrated high levels of damage in past earthquakes (see photos in Figure 1.1, described further in **STREST Deliverable 2.3**) are used as an application of the guidelines. Damage to these buildings can affect the structural system, the non-structural components (such as the external cladding), and the contents of the building, thus leading to a number of direct economic losses and the time required to repair the damage leads to additional business interruption losses.

Figure 1.1: Some photos of damage to precast industrial warehouse buildings due to earthquakes including column rotation failure, cladding failure, and beam-column connection failure

The second chapter of these guidelines provides recommendations for modelling seismic hazard in Europe; the third chapter looks at the performance of buildings within industrial districts, and suggests methods for developing fragility functions for structural and non-structural components and contents (and an application of these guidelines to a specific set of structures is provided in Appendix A); the fourth chapter describes the requirements for modelling the consequences of damage with a focus on monetary losses; and the last chapter provides the framework for combining the components of hazard, performance and consequences assessment within a probabilistic risk model.

1.2 SOME KEY CONCEPTS USED IN THESE GUIDELINES

Structural fragility function: a relationship that provides the probability of exceedance of a set of structural limit states (related to increasing costs of repair/replacement), conditioned on a scalar ground-motion intensity level, for a given typology of building. The most common intensity measure type for low-rise industrial buildings is spectral acceleration at the yield period. The building-to-building variability (due to buildings of a given typology having different capacity characteristics) and record-to-record variability should be accounted for in the fragility functions.

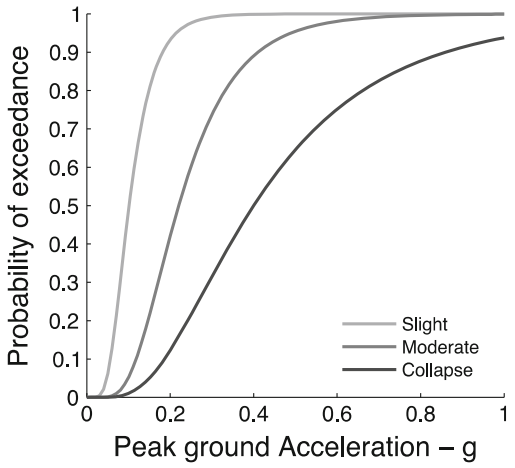

Figure 1.2: Example of structural fragility functions of a given building typology for three limit states, where the intensity measure type on the x axis is Peak Ground Acceleration (PGA)

Non-structural fragility function: a relationship that provides the probability of collapse of non-structural components (e.g. horizontal and vertical cladding and infill panels in industrial buildings), conditioned on a scalar ground motion intensity level, for a given typology of building. If the intensity measure type for non-structural elements is the same as that for structural elements, then this simplifies the probabilistic risk assessment, as discussed in Chapter 5.

Contents fragility function: a relationship that provides the probability of the need for replacement conditioned on a scalar ground motion intensity level. Typically the intensity measure type is peak floor acceleration.

Damage-loss model: the costs of repairing/replacing different damage states (structural, non-structural and contents) are needed for the structural, non-structural and contents

vulnerability functions. An estimation of the downtime costs related to building replacement (in the case of collapse or excessive residual drift) or structural and non-structural repair (for each damage state) are instead used for business interruption vulnerability functions.

Structural vulnerability function: a relationship that provides the mean loss ratio (mean ratio of cost of structural repair to cost of structural replacement), conditioned on a scalar ground motion intensity level, for a given typology of building – see Figure 1.3. The loss ratios are derived by combining the fragility functions with the damage-loss models at a number of levels of intensity. The repair cost variability should be accounted for through a coefficient of variation (CoV) applied to mean loss ratio (which could be defined following the recommendations of Porter, 2010 – see Figure 1.4).

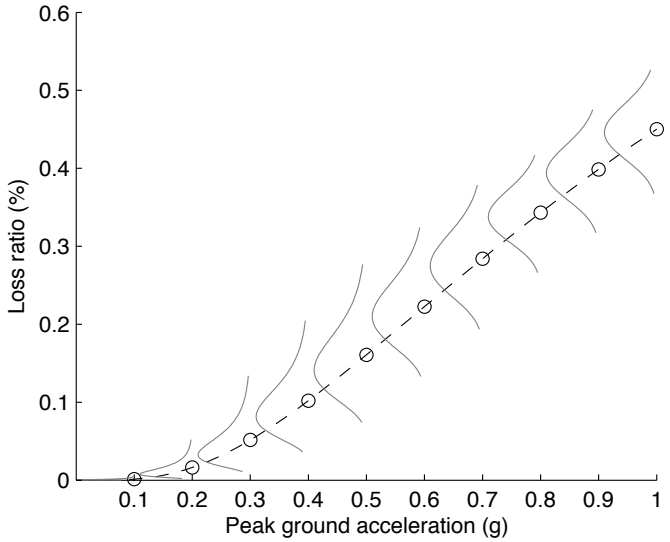

Figure 1.3: Example of a structural vulnerability function, where the intensity measure type on the x axis is Peak Ground Acceleration (PGA) and the mean and distribution of loss ratio is shown at discrete levels of PGA

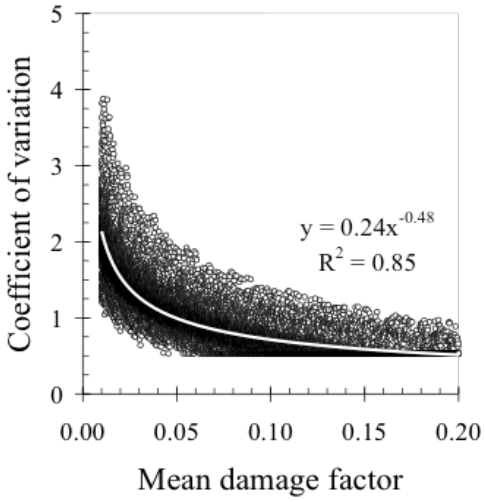

Figure 1.4: Coefficient of variation as a function of mean damage factor (i.e. mean loss ratio) from Porter (2010)

Non-structural vulnerability function: a relationship that provides the distribution of loss ratio (ratio of cost of non-structural repair to cost of non-structural replacement), conditioned on a scalar ground motion intensity level, for a given typology of industrial pre-cast building.

Contents vulnerability function: a relationship that provides the distribution of loss ratio (ratio of cost of contents repair to cost of contents replacement), conditioned on a scalar ground motion intensity level, for a given typology of industrial pre-cast building.

Business interruption vulnerability function: a relationship that provides the distribution of downtime (number of days to get back to full operations), conditioned on a scalar ground motion intensity level, for a given typology of industrial pre-cast building.

2 Guidelines for hazard modelling

In order to estimate the frequency and intensity characteristics of strong ground shaking due to earthquakes, at least one of each of the following models are needed:

- A seismological/source model that describes the location, geometry, and activity of seismic sources (described through magnitude-frequency distributions)
- A ground-motion model that describes the probability of exceeding a given level of ground motion at a site, conditioned on a set of event and path characteristics such as magnitude, style of rupture, site-to-source distance, Vs30.
- A site condition model that describes the characteristics of the soil at each site in the model, typically using values of Vs30.

The following sections provide recommendations on the available models that can be used (and where necessary, appropriately modified) for the purposes of preparing a hazard model for the risk assessment of industrial districts in Europe. Although a hazard model can be built with a single seismological, ground-motion and site condition model, it is recommended that logic trees are developed for each of these components, as discussed further in **STREST Deliverable 3.1**.

2.1 SEISMOLOGICAL/SOURCE MODEL

The EU-FP7 project “Seismic Hazard Harmonization in Europe” (SHARE, 2009–2013) has produced the latest state-of-the art European seismic hazard model as a result of a community-based probabilistic seismic hazard assessment (Woessner et al., 2015). Three alternative earthquake source models are available for Europe within this model:

- An area source model based on the definition of areal sources for which earthquake activity is defined individually.
- A kernel-smoothed, zonation-free stochastic earthquake rate model that considers seismicity and accumulated fault moment.
- A fault source and background model, based on the identification of large seismogenic sources using tectonic and geophysical evidence.

Each of these source models, as well as the raw datasets which have been used to develop them, is available from the European Facility for Earthquake Hazard and Risk portal (www.efehr.org).

The three models can be used separately in a probabilistic risk assessment, but it has been suggested by the SHARE consortium that they are combined in a logic tree (see Figure 2.1), with weights that vary as a function of the probability of exceedance level (Woessner et al., 2015) as some methods are more appropriate for defining the hazard at longer return periods (e.g. the use of slip rates on faults) whereas others provide a better insight into the short term hazard (e.g. the smoothing of seismicity from earthquake catalogues).

2.2 GROUND-MOTION MODEL

The SHARE consortium has also developed a ground-motion logic tree, as shown in Figure 2.1, for ground motion prediction equations (GMPE).

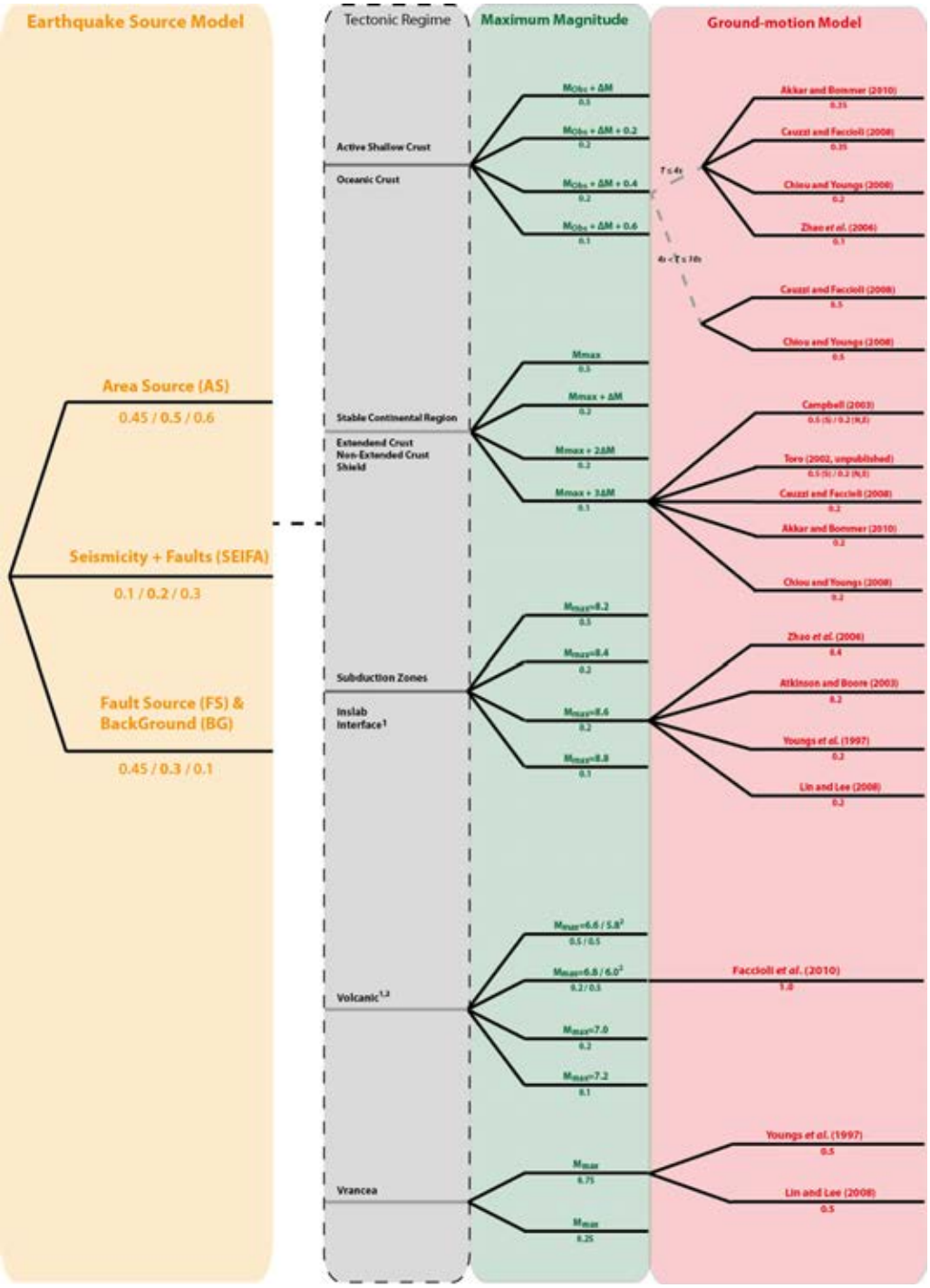

Figure 2.1. SHARE logic tree (Woessner et al., 2015). Colours depict the branching levels for the earthquake source models (yellow), maximum magnitude models (green) and ground motion models (red). Values below the black lines indicate the weights, for the source model these indicate the weighting scheme for different return periods. Tectonic regionalisation is not a branching level (grey) of the model, however, it defines the GMPEs to be used

It is recommended that ground motion models are first selected on the basis of their ability to predict the intensity measures used in the fragility functions (described further in Chapter 3). In general, it is sufficient to consider the spectral acceleration at the yield period of the structure and peak ground acceleration as intensity measures for the performance of structural/ non-structural components and contents, which all of the ground-motion models in Figure 2.1 are capable of estimating.

2.3 SITE CONDITION MODEL

An important aspect of industrial districts is that they are not concentrated at a single site, but can be spread across kilometres of land. The soil profiles beneath the buildings can vary significantly and the influence of the local site conditions on the amplification of ground shaking in the event of an earthquake needs to be taken into consideration in the model.

The methods recommended to account for the site conditions, described further in **STREST Deliverable 3.4**, depend on the availability of data for each building within the industrial district. Given the number of assets that need to be considered in a performance and consequence assessment of an industrial district, it is unlikely that a full site-specific assessment of the soil conditions influencing the hazard at each location will be possible. Hence, it is proposed to use the generic or partially site-specific methods described in Deliverable 3.4 (so-called Level 0 and Level 0.5), wherein the site effects are accounted for either through the ground-motion prediction equations (using an appropriate value of Vs30 at each site) or through amplification factors applied to the hazard on ground with a Vs30 of 800 m/s. The latter method requires additional measurements of Vs5, Vs10, Vs20 and Vs30 at each site. In both cases it should be considered that the inclusion of site effects in the GMPEs proposed by the SHARE consortium would lead to an increase in the epistemic uncertainty (compared to that in the current logic tree shown in Figure 2.1) due to the different site information used in each GMPE (site classes or continuous Vs30) and the fact that some models account for nonlinear effects in soft soils and others do not, as discussed further in Deliverable 3.4.

2.4 AFTERSHOCK HAZARD MODEL

Industrial districts have been subjected to cumulative damage in past earthquake events due to a succession of aftershocks (e.g. the Emilia earthquakes of May 2012). In order to include aftershocks, as discussed in Iervolino et al. (2014), it is necessary to use models such as Omori's law (Utsu, 1961) - which models primary aftershocks - or epidemic-type aftershock sequences (ETAS; e.g., Ogata, 1988) - wherein each event is able to generate its own sequence - when stochastically generating events for the risk assessment (as discussed further in Chapter 5).

3 Guidelines for fragility modelling

3.1 STRUCTURAL/NON-STRUCTURAL COMPONENTS

This section presents guidelines for developing structural and non-structural fragility functions for precast industrial buildings, for which there are few existing fragility functions. As buildings have been designed to different design codes in each country in Europe, their structural and non-structural fragility can vary significantly. For this reason, methods for developing new fragility functions are summarised in the next sections, and an application of these methods to Italian industrial precast buildings is provided in Appendix A. For other building types, fragility functions from the literature can be used (see e.g. Pitilakis et al., 2014).

3.1.1 Generation of structural/non-structural fragility functions

Fragility curves represent the probability of the structural/non-structural components reaching designated damage levels (defined in Section 3.1.4), given the level of ground motion intensity. The flowchart for the development of fragility functions is presented in Figure 3.1.

For each typology of industrial buildings, the details of at least 100 potential buildings should be generated (for stability in the results, given that Monte Carlo analysis is used) and three-dimensional numerical models for each should be developed, as described in Sections 3.1.2 and 3.1.3. For each model a number of non-linear dynamic analyses should then be performed using a set of ground motions, which should be selected as described in Section 3.1.5. The results of the dynamic analyses were then used to form a damage probability matrix, which presents, for each seismic event and corresponding intensity, a ratio of buildings per subclass that reached a certain damage state. Fragility curves can then be then developed using regression analysis (ideally using maximum likelihood regression, as described in (Baker 2014b) and (Baker 2014a)) on the cumulative percentage of buildings in each damage state for a set of intensity levels. A lognormal distribution can be assumed.

3.1.2 Modelling structural components

3.1.2.1 Characteristics

The first step to developing fragility functions for structural components is to identify and describe their main characteristics.

Typically in Europe, precast warehouse buildings consist of parallel portals, composed of beams placed on corbel connections at the top of the columns. Two common warehouse distributions are presented in Figure 3.2. A neoprene pad is usually inserted between the elements, and in some cases additional steel dowels are provided at the beam-column connection. Columns are fixed at the bottom by socket foundations. Parallel portals support a roof system, which is typically an assembly of precast elements (girders, TT slabs, hollow core slabs), which, in the case of a seismic event, generally does not behave as a rigid diaphragm (see (Magliulo et al. 2014), (Liberatore et al. 2013), (Casotto et al. 2015) and (Belleri et al. 2014)).

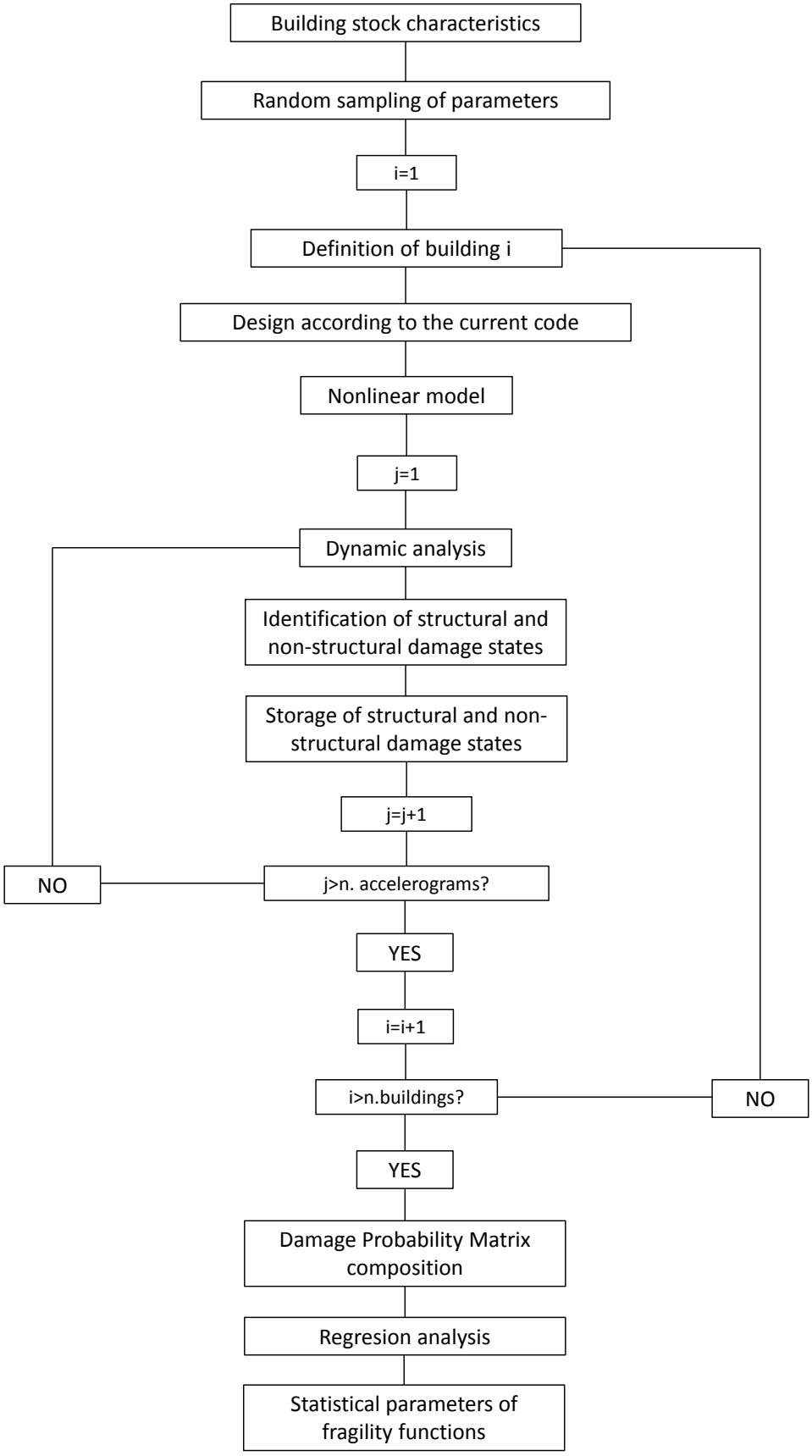

Figure 3.1: Fragility function derivation flowchart

The design code applied at the time of construction of a building class can also play a role in its response. Due to different requirements in regulations, the beam-to-column connections may depend only on friction, whereas additional dowels may be implemented in the connections of more modern buildings.

The building stock within the region of interest can be artificially generated by first obtaining information regarding material characteristics (e.g. concrete compressive strength, steel yield strength), geometry (e.g. beam length, span length, column height) and design load cases. These parameters can be considered as random variables, and Monte Carlo simulation used to develop a set of potential structures, each of which is designed based on the design code in place at the time of construction, such that sufficient information to numerically model each structure is obtained (Casotto et al. 2015). Appendix A presents examples of the data that has been collected and used to generate a set of industrial buildings typical of the construction in northern Italy.

Figure 3.2: Structural configuration of Italian precast warehouses (Casotto et al. 2015)

3.1.2.2 Numerical models

The proposed numerical model of structural components that can be used to represent the structural systems in Figure 3.2 is described herein. This model has been developed in the OpenSees finite elements platform (McKenna & Fenves 2010). The model consists of portals, connected by the roof system. Different non-structural elements can be attached to the portals using springs, which are added to the model in the form of zero-length elements. All the springs are independent one from another.

Each portal is composed of columns and beams (Figure 3.3). Columns are modelled by one component lumped plasticity elements. Plastic hinges at the bases of the columns are defined by the quadri-linear moment-rotation relationship, taking into account the pre-crack, post-crack and post-yield stiffness, as well as the negative linear post-capping stiffness. The characteristic rotations are determined according to a previous study (Dolsek 2010), whereas the characteristic moments are based on moment-curvature analysis using zero-length fibre section elements and the constant axial force from gravity load. Takeda hysteretic rules are applied. Beams are modelled as elastic elements connected to the columns by the contact zero-length elements based on Mohr-Coulomb frictional law, thus allowing the beams to slip from the columns, while considering interaction between accelerations in vertical and horizontal directions. The friction coefficient is taken from (Magliulo et al. 2011), whereas no cohesion is assigned. In addition to the contact element, an elastic no-tension spring with an initial gap is modelled between a column and a beam to

emulate the possible impact between the two elements. In the case of structures with dowels, this is modelled in each beam-to-column connection with an additional shear spring, which is removed from the model during the analysis, if the strength of the dowel is attained. The force-displacement relationship of the spring representing the dowel is determined according to (Zoubek et al. 2014). Masses are concentrated at the endpoints of the beams.

The roof system is modelled by truss elements, resulting in a flexible performance, which is in accordance with observations made after the earthquakes in Emilia Romagna (e.g., (Magliulo et al. 2014), (Liberatore et al. 2013) and (Belleri et al. 2014)).

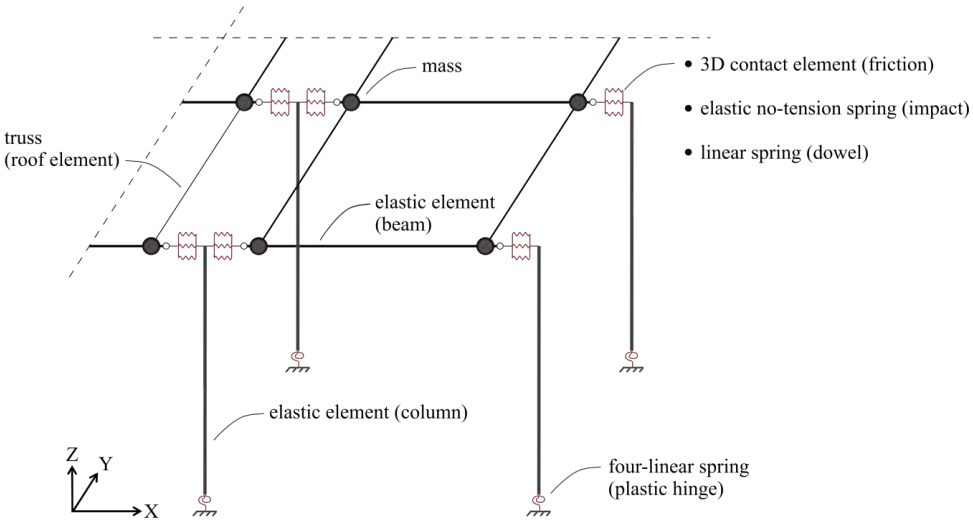

Figure 3.3: A schematic illustration of the proposed numerical model of structural components

3.1.3 Modelling of non-structural components

The non-structural components that lead to the most damage and loss in industrial buildings are the cladding elements. There are various types of claddings in precast buildings, with the most common being vertical precast panels, horizontal precast panels and concrete masonry infill panels, which are thus covered in these guidelines.

3.1.3.1 Vertical and horizontal panels

3.1.3.1.1 Characteristics of vertical and horizontal panels

Vertical and horizontal panels can be considered to be very stiff elements, attached, respectively, to the beams and columns (Isaković et al. 2012). The typical dimensions of the panels are needed, and they can be modelled as random variables (using the method described before for the geometry and material properties of the structure).

At the bottom, vertical panels are most often restrained to the foundation beam, whereas horizontal panels are generally placed on vertical supports (i.e. steel corbels), implemented into columns (Isaković et al. 2012). The corbels prevent vertical and out-of-plane horizontal displacements, but allow in-plane horizontal drifts to some extent, due to a gap provided for the installation of the panels. These drifts lead to friction between the corbels and the panel. Appendix A presents the assumptions that have been made to characterise the vertical and horizontal panels in Italian precast warehouses.

At the top of both vertical and horizontal panels, fastenings are typically provided to prevent overturning. Information on the typical fastening types in the country of interest should be sought, and Appendix A presents the data collected from the Italian construction market. Hysteretic rules for the considered fastenings are also needed, such as those given in Figure 3.4: . Appendix A provides more details on the calibration of these models for Italian buildings.

Openings can be considered in a simplified manner with the doors modelled in one direction (frames in the X direction) by taking out two panels in one of the bays. In the other direction (frames in the Y direction) windows can be considered by reducing the mass of the panels (Figure 3.5). The reduction factor can be determined on the basis of the glazed area, which can be treated as a random variable. The minimum and maximum fractions of the glazed area should be assessed on the basis of the information from producers in the country of interest.

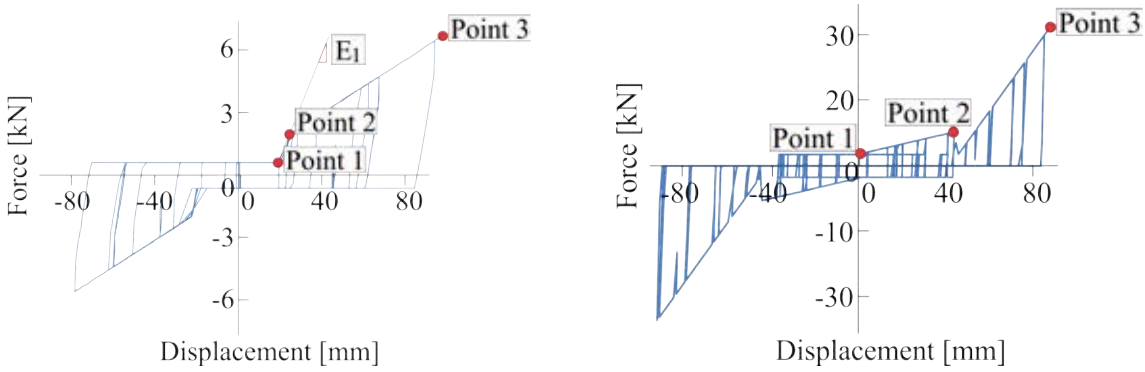

a) b)

Figure 3.4: a) Force-displacement relationships, modelled in OpenSees (McKenna & Fenves 2010) a) of a shear fastening and b) of a pinned fastening

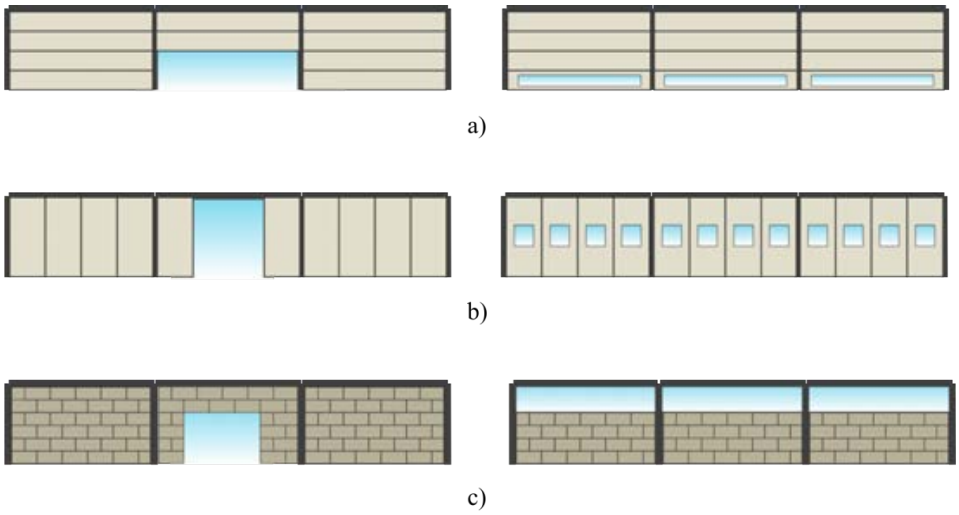

Figure 3.5: Location of openings in buildings with a) vertical panels, b) horizontal panels and c) masonry infills.

3.1.3.1.2 Numerical models

In the in-plane direction (parallel to the plane of the panels) vertical panels are modelled as springs connecting beams to fixed nodes (Figure 3.6), thus following the observations that the most significant deformations occur in the panel-to-structure connections (Liberatore et al. 2013). A non-linear relationship, typical for the sliding connections (Isaković et al. 2013), can be defined by combining different non-linear springs. The same model was used and described in (Babič & Dolšek 2014). In the out-of-plane direction (parallel to the plane of the panels) vertical panels can be modelled independently as nodal masses connected to the beams by linear springs.

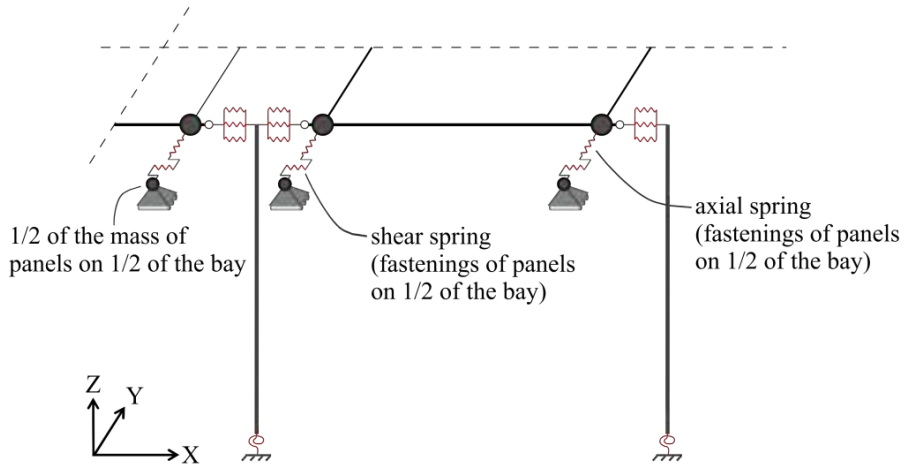

Figure 3.6: A schematic illustration of numerical model of a building with vertical panels.

Horizontal panels can be modelled by elastic elements with high stiffness, which are attached to the columns (Figure 3.7). The mass should be assigned at the centre of each panel. The vertical connections at the bottom (corbels) can be modelled as contact zero-length elements based on Mohr-Coulomb frictional law. Sliding of the panels is allowed in the in-plane direction, whereas displacements in the out-of-plane direction are prevented by an additional elastic spring. Moreover, the in-plane drifts are limited at the end of the gap provided for the panel installation by an additional elastic no-tension spring. At the top of each panel, panel-to-structure connections (either sliding or pinned) in the in-plane direction can be modelled by combining different non-linear springs (Figure 3.4:). The sliding connection can be modelled as described in (Babič & Dolšek 2014), whereas modelling of a pinned connection requires parallel binding of elastic perfectly-plastic materials and elastic perfectly-plastic materials with initial gaps. In the out-of-plane direction fastenings are modelled by an elastic spring with high stiffness displacements, which prevents displacements.

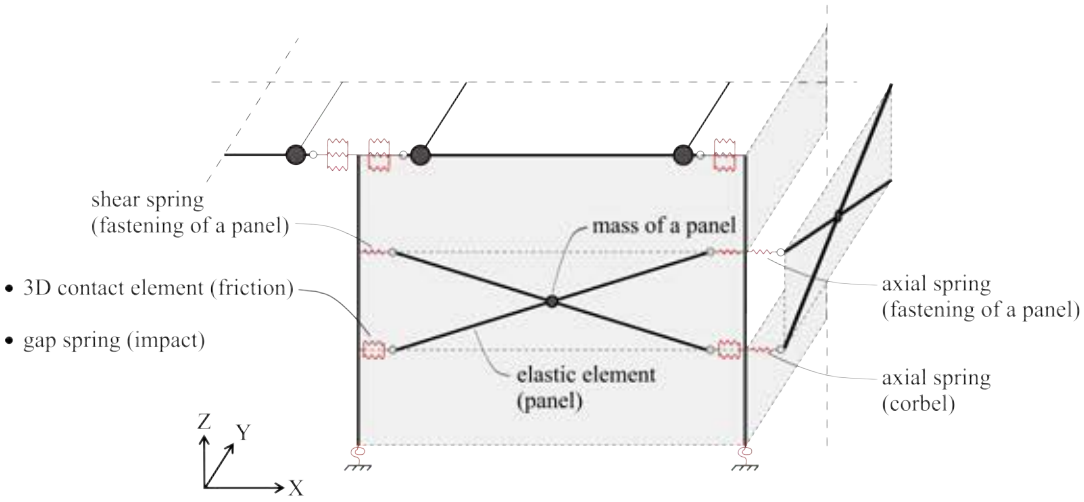

Figure 3.7: A schematic illustration of numerical model of a building with horizontal panels.

3.1.3.2 Masonry infills

3.1.3.2.1 Characteristics of masonry infills

Concrete masonry infills are usually situated between columns in industrial buildings. Distributions of the infill thickness, volumetric weight, shear modulus and shear strength are needed. Appendix A presents the data that was collected and assumed for the Italian building stock. In general it can be considered that infills have a poor connection with the adjacent beam, resulting in negligible vertical load being transmitted from the roof. If no out-of-plane restraints are provided as well, no arching mechanism is able to form and overturning of an infill can be prevented only by the self-weight of the infill and friction at the infill-to-column connection. Such failures were observed after recent Italian earthquakes (Belleri et al. 2014). The distribution of friction coefficient between infills and columns can be taken from (Aslam et al. 1980).

For the openings, assumptions based on the typical construction practices should be made. Appendix A presents the assumptions for the Italian building stock, together with the treatment of the window height as a random variable.

3.1.3.2.2 Numerical models of masonry infills

Masonry infills can be modelled by stiff elastic elements and zero-length elements (Figure 3.8). The mass should be concentrated at the centre of the infill. The infill-to-foundation connection can be modelled by two elastic no-tension springs, thus allowing rocking of the infill in the out-of-plane direction. Connections to the adjacent columns are modelled by the impact zero-length elements, which are able to capture frictional effects in the out-of-plane direction and impact in the in-plane direction. The latter is defined by the bi-linear force-displacement relationship, taking into account initial stiffness, crack deformation and post-crack stiffness according to (Panagiotakos & Fardis 1996) and (Fardis 1996). Openings are accounted for by reducing stiffness and strength of the infills as suggested in (Dawe & Seah 1988). Note that in buildings with masonry infills, an additional plastic hinge is placed at the infill-column joint at the top of the infill to capture the non-linear behaviour of the column.

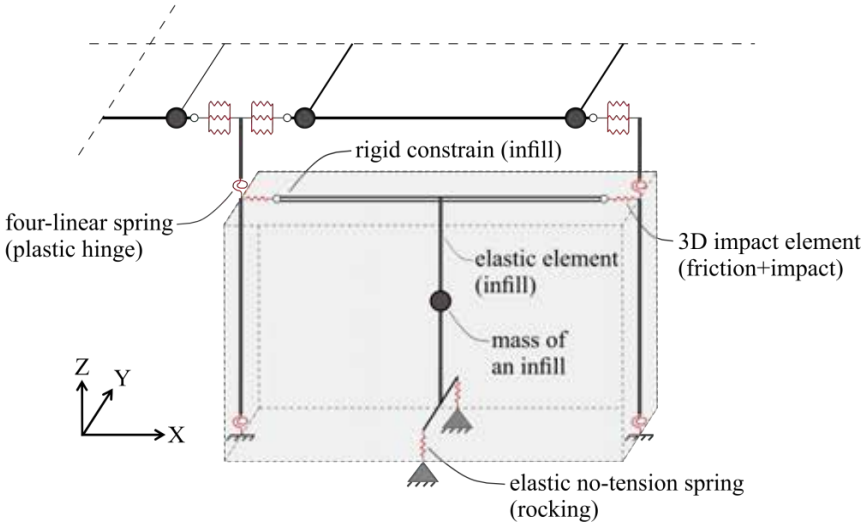

Figure 3.8: A schematic illustration of a numerical model of a building with masonry infills.

3.1.4 Definition of damage states

3.1.4.1 Structure damage states

Damage states of the bearing structures can be defined on the basis of qualitative descriptions found in (FEMA 2003), where damage is divided into four damage states (slight, moderate, extensive and complete) and is described for various types of structures. Since the typical European precast reinforced concrete buildings are not constructed in the USA, a different type of structures, with common characteristics (Precast Concrete Frames with Concrete Shear Walls) has been used as a reference for the damage scale proposed herein.

It is proposed that only three of the four damage states are taken from (FEMA 2003), i.e. moderate, extensive and complete. In addition, the *near complete* damage state is defined, which has the same damage-loss model for structural and non-structural components as the *complete* damage state, but a different impact on the damage of contents. For a detailed description of consequence functions the reader is referred to Section 4.

Moderate damage state

The moderate damage state is defined as a consequence of either of the following:

- Rotation in the plastic hinge of at least one column exceeds the yield rotation, taken from (Dolsek 2010).
- Friction capacity in at least one beam-to-column connection is exceeded (for buildings where dowels are not present).

Extensive damage state

Extensive damage state is defined as failure of at least one dowel connection. The strength of the connection can be assessed according to (Zoubek et al. 2014) (only in structures with dowel connections).

Near complete damage state

Near complete damage state is defined as a consequence of either of the following:

- Rotation in the plastic hinge of at least one column exceeds the ultimate rotation (CEN 2005), which corresponds to 80% of the strength, if measured in the post-capping range.
- Residual drift of at least one column exceeds 1.5%. This ultimate residual drift is equal to the median residual drift capacity from (Ramirez & Miranda 2012) .

Complete damage state

Complete damage state was defined as a consequence of either of the following:

- Dynamic instability of the structure.
- Unseating of at least one beam, which occurs if the relative beam drift exceeds the sliding capacity. The sliding capacity for buildings with friction connections can be taken as equal to the length of the corbel, which supports the beam. For buildings with dowel connections, the sliding capacity is smaller due to the end part of the corbel being torn away, when the failure of the dowel connection occurs. This reduction depends on the location of the dowel, which can be assumed on the basis of (Contegni et al. 2008).

3.1.4.2 Damage states of non-structural elements

Damage states of non-structural elements are defined at the level of a building by defining thresholds of the proportions of the collapsed non-structural elements in the building. Eleven damage states have been defined as presented in Table 1.

Table 1: Definition of damage states for non-structural components

Damage state	Description
DS1	At least one non-structural element dislocated
DS2	At least 10% of non-structural elements dislocated
DS3	At least 20% of non-structural elements dislocated
DS4	At least 30% of non-structural elements dislocated
DS5	At least 40% of non-structural elements dislocated
DS6	At least 50% of non-structural elements dislocated
DS7	At least 60% of non-structural elements dislocated
DS8	At least 70% of non-structural elements dislocated
DS9	At least 80% of non-structural elements dislocated
DS10	At least 90% of non-structural elements dislocated
DS11	All non-structural elements dislocated

Failure criteria for vertical and horizontal panels

It is assumed that the dislocation of vertical and horizontal panels occurs when the failure of panel-to-building connections (fastenings) is attained. Fastenings fail if either of the following two criteria is met:

- Exceedance of the ultimate displacement in the in-plane direction.
- Exceedance of the axial strength in the out-of-plane direction.

Failure criteria for masonry infills

The collapse of masonry infills occurs if either of the following two criteria is met:

- In-plane strength of the infill is exceeded.
- Critical infill rotation, representing overturning, is exceeded

In addition, it is assumed that dislocation of all the non-structural elements occurs if the building collapse or has to be demolished (i.e. has reached the *near complete* damage state).

3.1.5 Seismic input for regional fragility functions

Once numerical models have been developed of the structures and their non-structural components, nonlinear dynamic analysis is undertaken. As the fragility functions are to be used across large regions within a country, across which the characteristics of the hazard also vary, the records should not necessarily be matched to specific spectral shapes but should instead be chosen to cover the range of magnitudes and distances found within the hazard model, over the range of return periods used in the probabilistic risk model. The details of the records selected for the Italian buildings are provided in Appendix A.

3.1.6 Example fragility functions

Figure 3.9 presents an example of the resulting fragility functions for both structural and non-structural components, for all of the considered damage states.

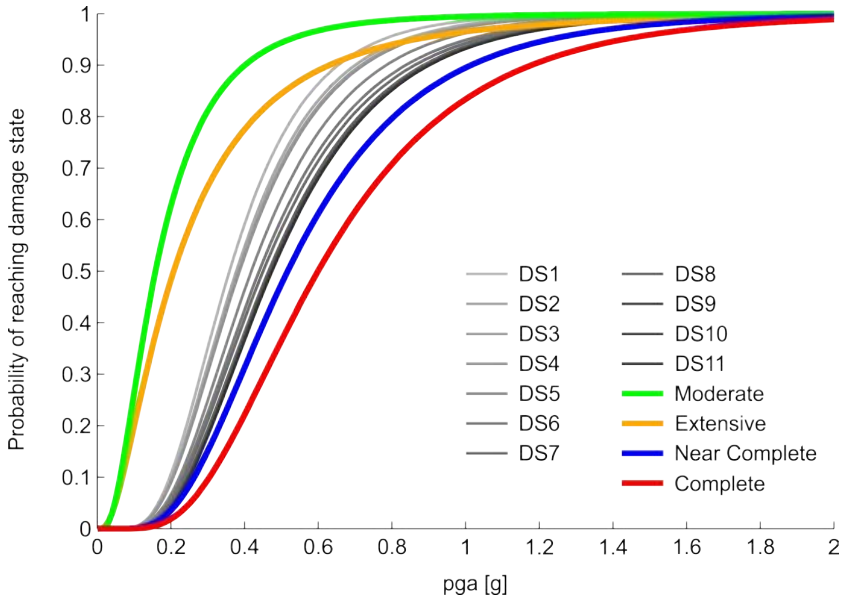

Figure 3.9: Example fragility functions for structural and non-structural components of industrial buildings

3.2 CONTENTS

This section provides guidelines on the modelling of contents of industrial warehouses, where the latter are those elements added by the owner following the construction and delivery of the building. As the fragility of contents can be considered to be standard across different countries in Europe, rather than propose methods for developing new contents fragility functions, these guidelines provide a set of proposed fragility functions. These guidelines have been based on the findings of the vulnerability consortium of the Global Earthquake Model[1] (Porter et al., 2012).

3.2.1 Categories of contents

The most commonly damaged contents in industrial buildings have been found by Porter et al. (2012) to be:

- Fragile stock and supplies on shelves
- Computer equipment
- Industrial racks
- Movable manufacturing equipment.

3.2.2 Damage states

Only one damage state is considered for contents, and the consequence of damage is that the contents must be replaced.

[1] http://www.globalquakemodel.org/what/physical-integrated-risk/physical-vulnerability/

3.2.3 Proposed fragility functions

A simplification of the procedure in ATC-58 (ATC, 2012) as proposed by Porter et al. (2012) is recommended herein for large industrial districts. The ATC-58 damage-analysis procedure provides component damage in discrete damage states using fragility functions derived from experiments, earthquake experience, first principles and, in some cases, expert judgment. Porter et al. (2012) have taken the fragility functions from ATC-58 that most closely fit the contents typologies described above, leading to the lognormal distribution parameters given in Table 2. In some cases the restraint of the contents (poor, moderate or superior) can also be accounted for. The intensity measure type in all cases is peak floor acceleration (in g), which in the case of single storey industrial buildings can be taken as the peak ground acceleration.

Table 2: Content fragility parameter values

Content Category	Intensity Measure	Median (g)	Dispersion
Stock and supplies on shelves	Peak floor acceleration	Poor = 0.42 Moderate = 0.60	Poor = 0.4 Moderate = 0.6
Computer equipment	Peak floor acceleration	Poor = 0.40 Superior = 1.0	0.5
Industrial racks	Peak floor acceleration	0.42	0.4
Movable equipment	Peak floor acceleration	Poor = 0.9 Superior = 2.0	Poor = 0.4 Superior = 0.2

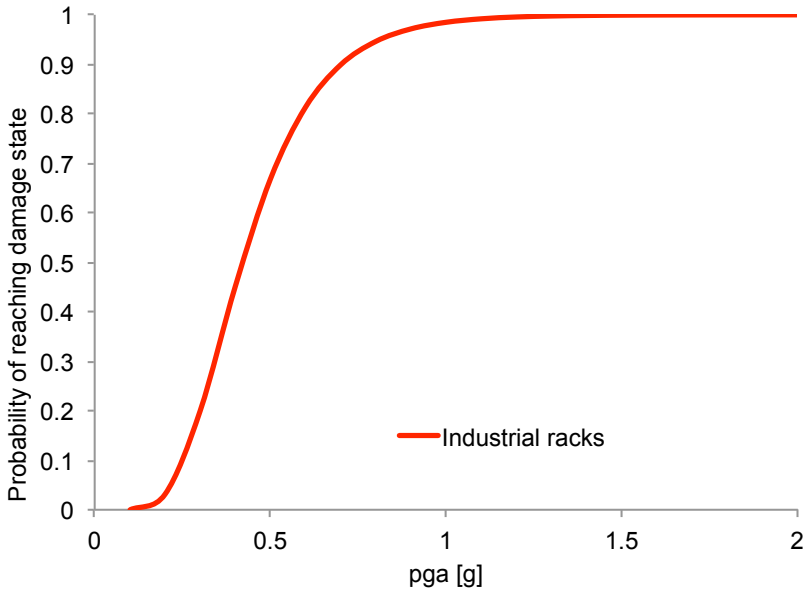

Figure 3.10: Example of the contents fragility function for industrial racks

4 Guidelines for loss modelling

Once fragility functions for structural/non-structural components and contents have been developed, the next stage is to transform these into vulnerability functions, which describe the probability of loss conditioned on a level of ground shaking. This is done through damage-loss models, as presented in this section.

4.1 DAMAGE-LOSS MODELS FOR STRUCTURAL/NON-STRUCTURAL COMPONENTS

4.1.1 Structural components

The damage-loss model for structural components is defined by damage factors corresponding to designated damage states. Damage factors in this case refer to the portion of construction cost of the bearing structure (without non-structural components) that is required to repair the damage state.

For the definition of *moderate*, *extensive* and *complete* damage state we refer here to (FEMA 2003) despite the fact that this exact type of structures cannot be found in the USA. Instead, a different structural type with common characteristics (Precast Concrete Frames with Concrete Shear Walls) is used to link physical damage obtained from numerical analyses to the damage ratios given by the aforementioned document.

Additionally, *near complete* damage state is defined in order to differentiate between the consequences of different structural damage states on contents. Explanation on how to integrate this dependence is given in Section 4.2. Also, the mean damage factors corresponding to near complete and complete damage states are increased by 10%, in order to account for extra costs related to demolition and removal of the ruins. The description of the damage states, their consequence and mean damage factors are given in Table 3.

Table 3: Description of damage-loss model for structural components

Damage state	Description	Consequences	Mean damage factor
Moderate	Yield capacity exceeded, observable movement at connections	Damaged structural components need to be repaired, whilst non-structural components and contents are not affected by the structural damage	10%
Extensive	Failure of some connections	Damaged structural components need to be repaired, whilst non-structural components and contents are not affected by the structural damage	50%

Near complete	Building did not collapse, but is damaged to the point where it needs to be demolished	Structural and non-structural components are lost, whilst contents are not affected by the structural damage	110%
Complete	Building fully or partially collapsed	All structural components, non-structural components and contents are lost	110%

To account for the impact that building collapse has on damage probability of contents, we write Equation 1:

$$\begin{aligned} P\left[DS_{cont} \geq ds_{i,cont}\right] \\ = P\left[DS_{cont} \geq ds_{i,cont} | DS_{str} = ds_{com,str}\right] \cdot P\left[DS_{str} = ds_{com,str}\right] \\ + P\left[DS_{cont} \geq ds_{i,cont} | DS_{str} \neq ds_{com,str}\right] \cdot P\left[DS_{str} \neq ds_{com,str}\right] \end{aligned} \quad (1)$$

Expression $P\left[DS_{cont} \geq ds_{i,cont}\right]$ refers to prior probability of contents damage state DS_{cont} reaching damage state $ds_{i,cont}$ and $P\left[DS_{struct} = ds_{com,struct}\right]$ refers to probability of structural damage state DS_{struct} reaching complete damage state of structural components $ds_{com,struct}$. Probability $P\left[DS_{str} \neq ds_{com,str}\right]$ equals $1 - P\left[DS_{str} = ds_{com,str}\right]$. Now we make an assumption that damage states of structural components and contents are statistically independent, i.e., if contents are placed outside the building, collapse of the building will not affect damage state of the contents. This implies that there is no correlation between ground motions, which cause structural collapse, and ground motions, which affect damage state of the contents. This seems rational, since structure is usually responsive to different characteristics of ground motions than contents. Under this assumption, Equation 2 holds.

$$\begin{aligned} P\left[DS_{cont} \geq ds_{i,cont} | DS_{str} = ds_{com,str}\right] = P\left[DS_{cont} \geq ds_{i,cont} | DS_{str} \neq ds_{com,str}\right] \\ = P\left[DS_{cont} \geq ds_{i,cont}\right] \end{aligned} \quad (2)$$

Now, we account for the fact that collapse of the building causes complete damage of the contents simply because contents are stored inside the building. Consequently, Equation 3 holds for all contents damage states $ds_{i,cont}$.

$$P'\left[DS_{cont} \geq ds_{i,cont} | DS_{str} = ds_{com,str}\right] = 1 \quad (3)$$

Posteriori probability $P'\left[DS_{cont} \geq ds_{i,cont}\right]$ can then be determined with Equation 4.

$$P'\left[DS_{cont} \geq ds_{i,cont}\right] = P\left[DS_{str} = ds_{com,str}\right] + P\left[DS_{cont} \geq ds_{i,cont}\right] \cdot P\left[DS_{str} \neq ds_{com,str}\right] \quad (4)$$

Equation 4 is considered when developing vulnerability models for contents, by combining the fragility functions with the damage-loss models.

4.1.2 Non-structural components

The damage-loss model for non-structural components is defined by damage factors corresponding to designated damage states. Damage factors in this case refer to the portion of construction cost of the non-structural components required to repair the damage. Such an approach seems relatively straightforward as the damage states are defined in such a way that their physical meaning is not as ambiguous as in the case of structural damage states. That is, the assumption that the increase of dislocated non-structural components proportionally increases the mean damage factors seems rational.

Due to extra costs related to removal of the dislocated components, extra expenditure may be included in the calculation and a 10% increase is assumed. The mean damage factors are presented in Table 4. If the structure collapses, then the damage factor for non-structural elements is assumed to be equal to that given for DS11.

Table 4: Description of damage-loss model for non-structural components

Damage state	Mean damage factor
DS1	6%
DS2	17%
DS3	28%
DS4	39%
DS5	50%
DS6	61%
DS7	72%
DS8	83%
DS9	94%
DS10	105%
DS11	110%

4.2 DAMAGE-LOSS MODEL FOR CONTENTS

Since there is only one damage state for each component and the consequence of damage is that the component must be replaced, the mean damage factor is 100%. If the structure collapses, then the damage factor for contents is assumed to be 100%.

4.3 DAMAGE-LOSS MODEL FOR BUSINESS INTERRUPTION

Business interruption (or downtime) is defined herein as the time needed to repair building damage, and has been divided into the following two components, following the recommendations of Mitrani-Reiser (2008) and Terzic et al. (2015):

- Mobilisation time (i.e. the time to undertake damage assessment, consultations with professional engineers, the contractor bidding process, debris clean-up, financing, contractor mobilisation etc. that needs to be completed before repairs can begin).
- Repair time (i.e. the time to return the structure to its pre-earthquake condition).

The financial loss due to this time may arise due to the loss in income from renting the damaged facility or the loss of daily revenue of the business. Additionally, in the case that the owner of a business is located in the facility, additional losses due to relocation cost and renting of new facilities may need to be considered. The potential sources of loss will need to be assessed on a case-by-case basis and used to define the business interruption value in the exposure model.

Given the damage states defined in Section 3.1.4, it is expected that building and business owners will consult with local contractors to estimate the mobilisation and repair time. Given that these are uncertain quantities, both the mean and dispersion values will need to be estimated, based on empirical data, literature review of past case studies and expert judgement. These times will depend on the extent of damage, and so will be needed for each structural and non-structural damage state, as illustrated in Table 5. In this case, the non-structural damage has been grouped into macro groups (≤ DS5 and >DS5). For both near collapsed and collapsed buildings, demolition and replacement will be required and so the downtime will be a direct function of the time to demolish and replace the building.

Table 5: Table of mobilisation and repair times per level of damage, for industrial precast RC buildings

Damage state	Mobilisation actions	Repair actions	Mean Downtime	Dispersion Downtime
No damage (structural or non-structural)	N/A	N/A	0	0
Moderate structural damage and ≤ DS5 non-structural damage	Detailed inspection, re-issuing drawings, permitting, clean-up, site preparation, financing, contractor/material	Column repair, beam-column friction connection repair (if present) and replacement of	TBD	TBD

	mobilisation	cladding/infill		
Moderate structural damage and > DS5 non-structural damage	Detailed inspection, re-issuing drawings, permitting, clean-up, site preparation, financing, contractor/material mobilisation	Column repair, beam-column friction connection repair (if present) and replacement of cladding/infill	TBD	TBD
Extensive structural damage and ≤ DS5 non-structural damage	Detailed inspection, re-issuing drawings, permitting, clean-up, site preparation, financing, contractor/material mobilisation	Column repair, beam-column dowel connection repair and replacement of cladding/infill	TBD	TBD
Extensive structural damage and > DS5 non-structural damage	Detailed inspection, re-issuing drawings, permitting, clean-up, site preparation, financing, contractor/material mobilisation	Column repair, beam-column dowel connection repair and replacement of cladding/infill	TBD	TBD
Near complete	-	-	Demolition and Replacement time	TBD
Complete	-	-	Demolition and Replacement time	TBD

Table 6 presents an example of median downtimes for buildings with moderate structural damage and ≤ DS5 non-structural damage, based on values suggested in Terzic et al. (2015). As illustrated in Figure 4.1, some of these activities can take place in parallel and so this should be taken into account when estimating the total median downtime due to mobilisation. The total repair time estimate is also dependent on the repair scheme preferred by the building owner, which could either be a slow-track repair scheme (components are repaired serially) and a fast-track repair scheme (components are repaired in parallel).

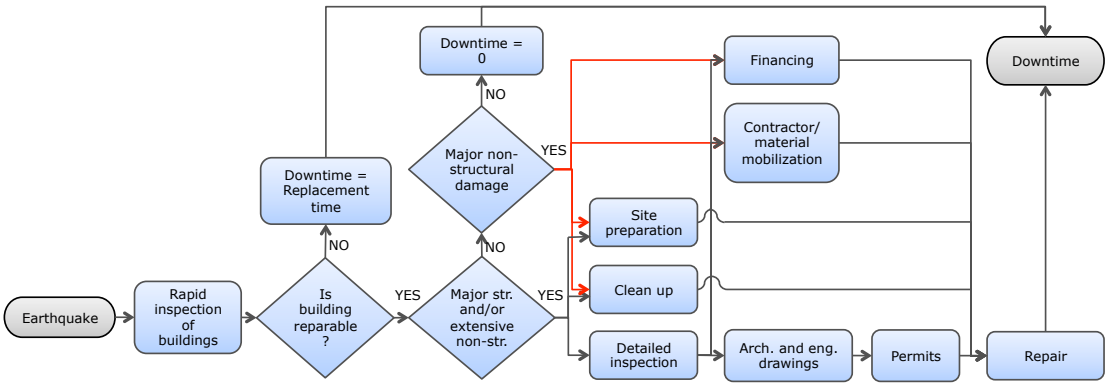

Figure 4.1: Mobilisation and repair activities that contribute to business downtime (Terzic et al., 2015)

Table 6: Illustration of median mobilisation downtimes for buildings with moderate structural damage and ≤ DS5 non-structural damage

Damage state	Median Downtime
Detailed inspection	2 weeks
Reissuing drawings	3 months
Permitting	1 month
Clean up	2 weeks
Site preparation	1 week
Financing	3 months
Contractor/material mobilisation	1 month

5 Guidelines for probabilistic multi-site loss assessment

5.1 HAZARD

Industrial districts comprise a number of structures that are distributed over large regions. The outputs of standard probabilistic seismic hazard assessment (i.e. hazard curves) cannot be used to assess the aggregated losses to portfolios of structures and instead a modified procedure is required as outlined below.

The seismological/source model (see Section 2.1) can be used to produce stochastic event sets, which are synthetic catalogues of potential earthquake ruptures obtained from Monte Carlo simulation (see e.g. Musson, 1999). Each event in the synthetic catalogue can then be used to generate a ground-motion field, which will be calculated using the logarithmic mean from the GMPE plus a random selection of the inter-event residual for the event and then a random selection of the intra-event residual for each site in the model (see e.g. Crowley and Bommer, 2006; Park et al., 2007).

The spatial correlation of the intra-event residuals should be accounted for when sampling this variability at each site in the loss model. A number of spatial correlation models that are a function of the separation distance between sites have been proposed (e.g. Wang and Takada, 2005; Goda and Hong, 2008; Goda and Atkinson, 2009; Jayaram and Baker, 2009), with some specifically based on European ground motion data (Esposito and Iervolino, 2011; 2012).

If different intensity measure types are used for the structural/non-structural components and/or contents (for example, Sa(1.0s) for the structural components, Sa(0.5s) for the non-structural components and PGA for the contents), then a spectral cross-correlation model is also needed to ensure that the residuals between the different intensity measure types are adequately correlated (e.g. Baker and Cornell, 2006). Weatherill et al. (2015) present various options for modelling both spatial correlation and spectral cross-correlation, and recommend the use of either full block cross-correlation (Oliver, 2003) or the linear model of co-regionalisation (Loth and Baker, 2013).

In order to avoid the additional computational effort required to develop spatially cross-correlated ground motion fields, the same intensity measure types should be used for all components of the loss model, and spatial correlation alone should be considered. The SHARE seismological models (see Section 2.1) are available as input to the OpenQuake-engine, an open source software for probabilistic seismic hazard and risk assessment (Pagani et al., 2014), which can be used to generate spatially correlated ground-motion fields. Future versions of this software are expected to also include spatial cross-correlation.

5.2 EXPOSURE AND VULNERABILITY

The exposure model that is needed for a probabilistic multi-site loss assessment for industrial buildings, as recommended herein, should include the following information for each industrial facility in the portfolio:

- Coordinates;
- ID to define industrial facility category in terms of structural type, non-structural type, and contents type (which will be linked to the vulnerability functions);
- Structural replacement cost;
- Non-structural components replacement cost;
- Contents replacement cost;
- Business interruption cost.

An example of an industrial facility category would be modern RC precast frames with dowel connections (structural type), with horizontal cladding (non-structural type), and with industrial racks and movable equipment (contents type).

Four vulnerability functions need to be defined for each industrial facility category and these are produced by combining the fragility functions (see Section 3) with the damage-loss models (see Section 4).

To produce structural vulnerability models, for a number of levels of ground shaking intensity, the probability of being in each damage state is estimated from the fragility functions (see Figure 5.1) and each probability is multiplied by the mean damage factors presented in Table 3 and summed to produce a mean loss ratio. A coefficient of variation (CoV) can be added to each mean loss ratio based on recommendations of Porter (2010), as outlined in Porter et al. (2012). The conditional distribution of structural loss ratio can be taken as a lognormal distribution with mean and coefficient of variation as described, or as a beta distribution with bounds of 0 and 1 and the same mean and coefficient of variation.

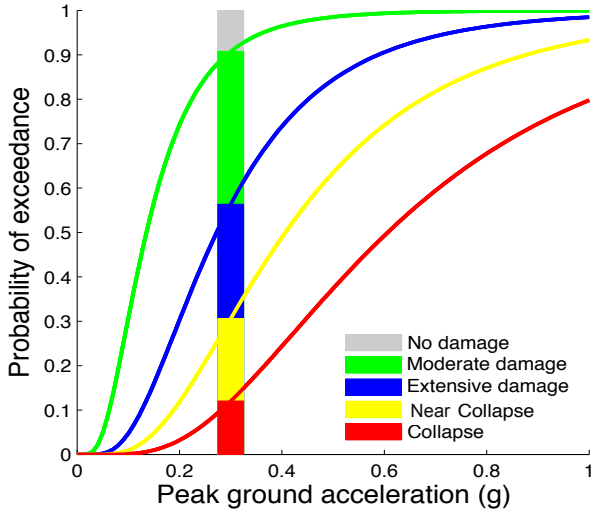

Figure 5.1: Probability of being in each damage state at a given level of ground shaking intensity

To produce non-structural vulnerability models, for each level of ground shaking intensity, the probability of being in each non-structural damage state (from the non-structural fragility functions) is multiplied by the mean damage factor for loss for non-structural elements (Table 4), and summed to produce a mean loss ratio. As above, a coefficient of variation (CoV) can be added to each mean loss ratio based on recommendations of Porter (2010). The conditional distribution of non-structural loss ratio can be taken as a lognormal distribution with mean and coefficient of variation as described, or as a beta distribution with bounds of 0 and 1 and the same mean and coefficient of variation.

To produce contents vulnerability models, it may be necessary to combine fragility functions for different types of contents. In order to do this it is necessary to know the percentage of each content type within the industrial facility category (in terms of replacement value). For example, if 80% of the contents value is from industrial racks and 20% is from movable equipment, then the fragility functions for these two contents types should be combined with these proportions. As discussed in Section 4.1, the vulnerability function for contents depends on whether the structure collapses or not. From equation 4, for each level of ground shaking intensity, the probability of collapse (from the structural fragility functions) is multiplied by the mean damage factor for contents (equal to 100%) and is added to the probability the structure does not collapse, multiplied by the combined fragility function, multiplied by the mean damage factor for contents (equal to 100%). As above, a coefficient of variation (CoV) can be added to each mean loss ratio based on recommendations of Porter (2010). The conditional distribution of contents loss ratio can be taken as a lognormal distribution with mean and coefficient of variation as described, or as a beta distribution with bounds of 0 and 1 and the same mean and coefficient of variation.

To produce business interruption vulnerability functions, for a number of levels of ground shaking intensity, the probability of being in each damage state in Table 5 (from the fragility functions) is multiplied by the associated mean downtimes and summed. The variance in the downtime at each intensity level can be obtained by summing the weighted variances. The conditional distribution of business interruption can be taken as a lognormal distribution with mean and variance as described, or as a beta distribution with bounds of 0 and 1 and the same mean and variance.

5.3 LOSS EXCEEDANCE CURVES

The output of a probabilistic multi-site loss assessment is a loss exceedance curve. Once stochastic event sets and associated ground-motion fields (for each event) have been computed, the intensity measure level at a given site in the exposure model is used to extract the loss ratio from each vulnerability function that has been defined for the industrial facility at that site. The loss ratios that are sampled for assets of a given taxonomy industrial facility category at different sites can be considered to be either independent or fully correlated. The latter case might be chosen, for example, when all facilities have been constructed by the same contractor. The losses for a given industrial facility are calculated using all of the ground-motion fields, leading to list of events and associated structural/non-structural/contents loss ratios and downtime. The loss ratios and downtime are multiplied by the value of each specified in the exposure model and summed to give a total loss for the facility. For a given industrial facility, this list is then sorted from the highest loss to the lowest. The rate of exceedance of each loss is calculated by dividing the number of exceedances of that loss by the total length of the stochastic event sets (in years). In the

case where aftershocks are not included in the event sets, it is possible to assume a Poissonian distribution of the earthquake occurrence model and calculate the probability of exceedance of each loss accordingly.

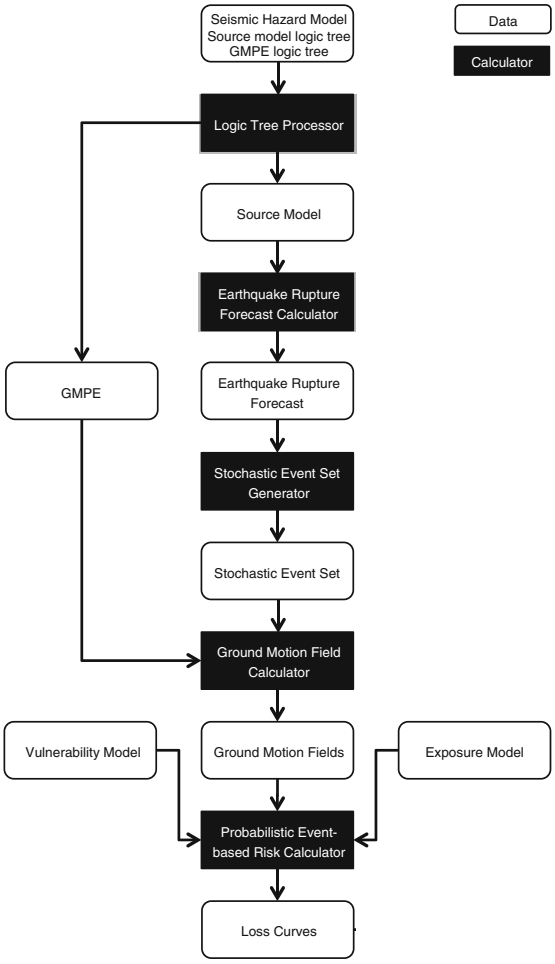

Figure 5.2. Workflow for developing loss exceedance curves

If an aggregate loss curve for the whole portfolio of industrial facility is required, it is necessary to sum the losses from all the industrial facility in the exposure file, per event, before calculating the exceedance frequency of loss.

All of these calculations can be done with the OpenQuake-engine, as described further in Silva et al. (2013) and Crowley and Silva (2013).

Figure 5.3 shows example loss exceedance curves and how various assumptions on the correlation of ground shaking residuals (as discussed in Section 5.1) can influence the losses, especially those at low frequencies of exceedance (i.e. high return periods).

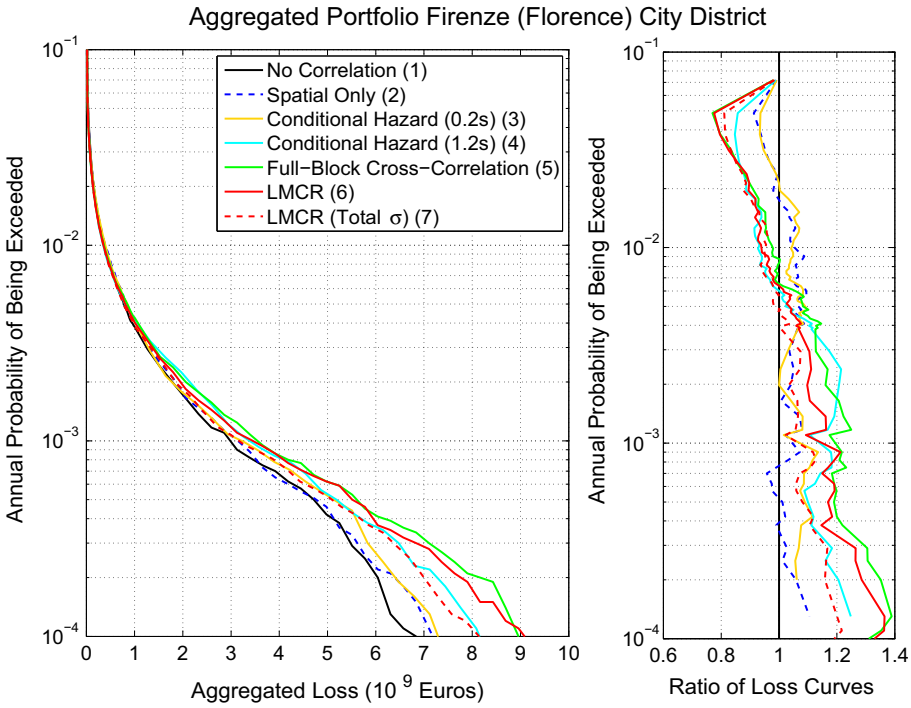

Figure 5.3: Example loss exceedance curves with different correlation models for the ground shaking residuals (Weatherill et al., 2015)

References

Aslam, M., Scalise, T. & Godden, W.G., 1980. Earthquake Rocking Response of Rigid Bodies. *Journal of the Structural Division*, 106(2), pp.377–392. Available at: http://cedb.asce.org/cgi/WWWdisplay.cgi?9293.

(ATC) Applied Technology Council, 2012. ATC-58: Guidelines for Seismic Performance Assessment of Buildings, 100% Draft. Redwood City, CA.

Babič, A. & Dolšek, M., 2014. The impact of structural components on fragility curves of single-storey industrial precast structures. In *Second European conference on earthquake engineering and seismology*. 1107. Istanbul, Turkey, pp. 1–12.

Baker, J.W., 2014a. Code supplement to efficient analytical fragility function fitting using dynamic structural analysis. Available at: http://purl.stanford.edu/sw589ts9300 [Accessed January 15, 2015].

Baker, J.W., 2014b. Efficient analytical fragility function fitting using dynamic structural analysis. *Earthquake Spectra In-Press*. Available at: http://earthquakespectra.org/doi/abs/10.1193/021113EQS025M.

Baker, J.W., Cornell, C.A. 2006. Correlation of response spectral values for multicomponents of ground motion. *Bulletin of the Seismological Society of America* 96(1): 215–227

Belleri, A. et al., 2014. Seismic performance of precast industrial facilities following major earthquakes in the Italian territory. *Journal of Performance of Constructed Facilities (in press)*. Available at: http://dx.doi.org/10.1061/(ASCE)CF.1943-5509.0000617.

Bournas, D.A., Negro, P. & Taucer, F.F., 2013. Performance of industrial buildings during the Emilia earthquakes in Northern Italy and recommendations for their strengthening. *Bulletin of Earthquake Engineering*, 12(5), pp.2383–2404. Available at: http://link.springer.com/article/10.1007/s10518-013-9466-z.

Casotto, C. et al., 2015. Seismic fragility of Italian RC precast industrial structures. *Engineering Structures (in press)*.

CEN, 2004a. *Eurocode 2: Design of concrete structures - Part 1-1: General rules and rules for buildings*, Brussels: European Committee for Standardisation.

CEN, 2004b. *Eurocode 8: Design of structures for earthquake resistance - Part 1: General rules, seismic actions and rules for buildings*, Brussels: European Committee for Standardisation.

CEN, 2005. *Eurocode 8: Design of structures for earthquake resistance - Part 3: Assessment and retrofitting of buildings*, Brussels: European Committee for Standardisation.

Colombo, A., Negro, P. & Toniolo, G., 2014. The influence of claddings on the seismic response of precast structures: The Safecladding project. In *Second European conference on earthquake engineering and seismology*. 1877. Istanbul, Turkey, pp. 1–12.

Contegni, M.M., Palermo, A. & Toniolo, G., 2008. *Strutture prefabbricate: Schedario di edifici prefabbricati in C.A.*, DPS/RELUIS. Available at: http://www.reluis.it/images/stories/Schedario edifici prefabbricati in ca.pdf.

Crowley, H. and Bommer, J.J., 2006. Modelling seismic hazard in earthquake loss models with spatially distributed exposure, *Bulletin of Earthquake Engineering,* 4(3)*,* 249-273

Crowley, H., Silva, V. 2013. OpenQuake Engine Book: Risk v1.0.0. GEM Foundation, Pavia, Italy.

Dawe, J.L. & Seah, C.K., 1988. Lateral load resistance of masonry panels in flexible steel frames. In *Proceedings of the Eighth International Brick and Block Masonry Conference*. Dublin, Republic of Ireland.

Dolsek, M., 2010. Development of computing environment for the seismic performance assessment of reinforced concrete frames by using simplified nonlinear models. *Bulletin of Earthquake Engineering*, 8(6), pp.1309–1329. Available at: http://link.springer.com/10.1007/s10518-010-9184-8 [Accessed November 5, 2014].

Esposito, S., Iervolino, I. 2011. PGA and PGV spatial correlation models based on European multievent datasets. *Bulletin of the Seismological Society of America* 101(5):2532–2541

Esposito, S., Iervolino, I. 2012. Spatial correlation of spectral acceleration in European data. *Bulletin of the Seismological Society of America* 102(6):2781–2788

Fardis, M.N., 1996. *Experimental and numerical investigations on the seismic response of RC infilled frames and recommendations for code provisions* M. N. Fardis, ed., Lisbon: Laboratorio Nacional de Engenharia Civil.

FEMA, 2003. *HAZUS-MH technical manual*, Washington, D.C.: Federal Emergency Management Agency.

Goda, K., Atkinson, G.M. 2009. Probabilistic characterisation of spatial correlated response spectra for earthquakes in Japan. *Bulletin of Seismological Society of America* 99(5): 3003–3020

Goda, K., Hong, H.P. 2008. Spatial correlation of peak ground motions and response spectra. *Bulletin of Seismological Society of America* 98(1): 354–365

Iervolino, I., Chioccarelli, E. & Convertito, V., 2011. Engineering design earthquakes from multimodal hazard disaggregation. *Soil Dynamics and Earthquake Engineering*, 31(9), pp.1212–1231. Available at: http://dx.doi.org/10.1016/j.soildyn.2011.05.001.

Iervolino, I., Giorgio M., Polidoro, B., 2014. Sequence-based probabilistic seismic hazard analysis, *Bulletin of the Seismological Society of America*, Vol. 104, No. 2, pp. 1006–1012.

Isaković, T. et al., 2012. *Improved fastening systems of cladding wall panels of precast buildings in seismic zones*, Ljubljana: University of Ljubljana.

Isaković, T. et al., 2013. *Report and card files on the tests performed on existing connections*, Ljubljana: University of Ljubljana.

Jayaram, N., Baker, J.W. 2009. Correlation model of spatially distributed ground motion intensities. *Earthquake Engineering and Structural Dynamics* 38:1687–1708

Liberatore, L. et al., 2013. Failure of industrial structures induced by the Emilia (Italy) 2012 earthquakes. *Engineering Failure Analysis*, 34, pp.629–647. Available at: http://dx.doi.org/10.1016/j.engfailanal.2013.02.009.

Loth, C., Baker, J.W. 2013. A spatial cross-correlation model of spectral accelerations at multiple periods. *Earthquake Engineering and Structural Dynamics* 42:397–417

Magliulo, G. et al., 2011. Neoprene-concrete friction relationships for seismic assessment of existing precast buildings. *Engineering Structures*, 33(2), pp.535–538. Available at: http://dx.doi.org/10.1016/j.engstruct.2010.11.011.

Magliulo, G. et al., 2014. The Emilia earthquake: Seismic performance of precast reinforced concrete buildings. *Earthquake Spectra*, 30(2), pp.891–912. Available at: http://www.earthquakespectra.org/doi/abs/10.1193/091012EQS285M [Accessed January 30, 2015].

Magrini, A., Martino, A. & Murano, G., 2011. *Trasmittanza termica*, Milano: Comitato Termotecnico Italiano Energia e Ambiente. Available at: http://www.iuav.it/Ateneo1/docenti/design-e-a/docenti-st/Romagnoni-/materiali-/energetica/abaco_pareti1.pdf.

McKenna, F. & Fenves, G.L., 2010. Open System for Earthquake Engineering Simulation (OpenSees). Available at: http://opensees.berkeley.edu.

Mitrani-Reiser J. 2008. Risk management products team downtime model, primary resource document for the FEMA P-58 Seismic Performance Assessment of Buildings, Methodology and Implementation series of products (see ATC, 2012)

MIT, 2009. *Circolare 2 febbraio 2009, n. 617 Istruzioni per l'applicazione delle «Nuove norme tecniche per le costruzioni» di cui al decreto ministeriale 14 gennaio 2008. (GU n. 47 del 26-2-2009 - Suppl. Ordinario n.27)*, Italy: Ministero delle Infrastrutture e dei Trasporti.

Musson, R.M.W., 1999. Probabilistic seismic hazard maps for the Balkan region, Annali di Geofisc. 42, no. 6, 1109–1124.

Ogata, Y. 1988. Statistical models for earthquake occurrences and residual analysis for point processes, J. Am. Stat. Assoc. 83, 9–27.

Oliver, D.S. 2003. Gaussian cosimulation: modelling of the cross-covariance. *Math Geol* 356: 681–698

Pagani, M., Monelli, D., Weatherill, G., Danciu, L., Crowley, H., Silva, V., Henshaw, P., Butler, L., Nastasi, M., Panzeri, L., Simionato, M. and Vigano, D., 2014. OpenQuake Engine: An open hazard (and risk) software for the Global Earthquake Model, *Seismological Research Letters*, Vol. 85, No. 3, pp 692-702

Panagiotakos, T.B. & Fardis, M.N., 1996. Seismic response of infilled RC frame structures. In *Proceedings of the Eleventh world conference on earthquake engineering*. Acapulco, Mexico.

Park, J., Bazzurro, P., Baker, J.W. 2007 Modeling spatial correlation of ground motion intensity measures for regional seismic hazard and portfolio loss estimation. In: Kanada, Takada, Furuta (eds) Applications of statistics and probability in civil engineering. Taylor and Francis Group, London

PEER, 2013. NGA strong motion database. Available at: http://peer.berkeley.edu/nga/ [Accessed July 18, 2013].

Pitilakis, K., Crowley, H., Kaynia, A, 2014. *SYNER-G: Typology definition and fragility functions for physical elements at seismic risk: buildings, lifelines, transportation networks and critical facilities*, Springer, Ed: Pitilakis, Crowley, Kaynia.

Porter, K. 2010. Cracking an open safe: uncertainty in HAZUS-based seismic vulnerability functions, Earthquake Spectra, 26 (3): 893-900

Porter K., Cho I. and Farokhnia K. 2012. Contents seismic vulnerability estimation guidelines, Available from URL: http://www.nexus.globalquakemodel.org/gem-vulnerability/posts/draft-content-vulnerability-guidelines

Ramirez, C.M. & Miranda, E., 2012. Significance of residual drifts in building earthquake loss estimation. *Earthquake Engineering & Structural Dynamics*, 41(July), pp.1477–1493. Available at: http://onlinelibrary.wiley.com/doi/10.1002/eqe.2217/full.

Regione Toscana direzione generale politiche territoriali, Il rischio sismico nelle aree produttive. , p.32. Available at: http://www.rete.toscana.it/sett/pta/sismica/01informazione/banchedati/edilizia_privata/img_ediliziaprivata/report_capannoni.pdf [Accessed February 2, 2015].

Silva, V., Crowley, H., Pagani, M., Monelli, D., Pinho, R. 2013. Development of the OpenQuake engine, the Global Earthquake Model's open-source software for seismic risk assessment. *Natural Hazards*, DOI: 10.1007/s11069-013-0618-x

STREST, 2014. Deliverable 2.3: Report on lessons learned from recent catastrophic events" www.strest-eu.org

STREST, 2014. Deliverable 3.1: Report on the effects of epistemic uncertainties on the definition of LP-HC events. www.strest-eu.org

STREST, 2014. Deliverables 3.4: Guidelines and case studies of site monitoring to reduce the uncertainties affecting site-specific earthquake hazard assessment. www.strest-eu.org

Terzic, V., Mahin, S.A., Comerio, M.C., 2015. Using PBEE in seismic design to improve performance of moment resisting frames by base-isolation, *Earthquake Spectra*, under review

Utsu, T., 1961. A statistical study on the occurrence of aftershocks, *Geophys. Mag*. 30, 521–605.

Verderame, G.M., Stella, A. & Consenza, E., 2001. Mechanical properties of reinforcing steel adopted in R.C. structures in the '60s. In *Proceedings of the 10th national ANIDIS conference: seismic engineering in Italy*. Potenza-Matera, Italy.

Wang, M., Takada T., 2005. Macrospatial correlation model of seismic ground motions. *Earthquake Spectra* 21(4):1137–1156

Weatherill, G., Silva, V., Crowley, H. & Bazzurro, P. 2015. Exploring the impact of spatial correlations and uncertainties for portfolio analysis in probabilistic seismic loss estimation, *Bulletin of Earthquake Engineering*, DOI 10.1007/s10518-015-9730-5

Woessner J., Danciu L., Giardini D., Crowley H., Cotton F., Grunthal G., Valensise G., Arvidsson R., Basili R., Demircioglu M., Hiemar S., Meletti C., Musson R., Rovida A., Sesetyan K. and Stucchi M, 2015. The 2013 European Seismic Hazard Model - Key Components and Results, *Bulletin of Earthquake Engineering,* DOI 10.1007/s10518-015-9795-1.

Zoubek, B., Fischinger, M. & Isaković, T., 2014. Estimation of the cyclic capacity of beam-to-column dowel connections in precast industrial buildings. *Bulletin of Earthquake Engineering (in press)*. Available at: http://link.springer.com/article/10.1007/s10518-014-9711-0.

A. Application of fragility functions guidelines

Three building classes can be used to describe about 90% of the reinforced concrete precast industrial buildings in the Tuscany database that is to be used in the case study application of the STREST test for industrial buildings in Work Package 6.

A description of the building classes addressed in this Appendix, along with other building classes of precast buildings, which are less typical for the Tuscan area, can be found in (Casotto et al. 2015).

This Appendix demonstrates the methodology and assumptions used to develop fragility functions for the industrial building stock in Northern Italy.

A.1. MODELLING OF STRUCTURAL COMPONENTS

A.1.1 Characteristics

Buildings in all the considered building classes consist of parallel portals, composed of beams placed on corbel connections at the top of the columns. A neoprene pad is usually inserted between the elements and, depending on the building class, additional dowels are provided. Columns are fixed at the bottom by socket foundations. Parallel portals support a roof system, which is an assembly of precast elements (girders, TT slabs, hollow core slabs), and, in the case of a seismic event, does not behave as a rigid diaphragm ((Magliulo et al. 2014), (Liberatore et al. 2013), (Casotto et al. 2015) and (Belleri et al. 2014)).

Buildings with type 1 structural configuration contain long saddle roof beams, whereas type 2 structural configuration is distinctive of buildings with shorter rectangular beams and larger distance between the portals (Figure 3.2). Depending on the time of construction, the code level of a building class is either pre-code or low-code for buildings built before or after 1996, respectively. Pre-code buildings were designed to withstand lateral load equal to 2 percent of the building self-weight, whilst design lateral load of low-code buildings, addressed in this document, amounted to 7 percent of the building self-weight. Moreover, due to different requirements in the design regulations it was assumed that beam-to-column connections in the pre-code buildings depended only on friction, whereas additional dowels were assumed to be implemented in the beam-to-column connections of the low-code buildings.

The building stock was generated by first obtaining information regarding material characteristics, geometry and design load cases and then designing them in compliance with the pre-code and low-code classification (Casotto et al. 2015). Material characteristics, geometric parameters and load cases are given in Table 8, Table 9 and Table 10, respectively. The differences between actual material characteristics and the values used in design were also considered. Thus, in the generation of the building stock values from Table 8 were taken. These values were obtained either from experimental campaign (Verderame et al. 2001) (Table 12) or by assuming an over-strength factor as stated in Table 13.

Furthermore, according to (Zoubek et al. 2014) the amount of stirrups in corbels and their configuration may have a critical influence on the dowel connection capacity. However, information regarding certain structural details is difficult to determine, since the codes did not provide instruction on how to design them. Design engineers may have relied on

different design guides or on their own engineering judgement, which is, by default, subjective. An effort was therefore made to implement a current approach and validate it on information accessible in field reports. Stirrups were designed according to strut-and-tie approach, which is implemented in EC2 (CEN 2004a). As a result the number of 8 mm stirrups in each corbel varied between 4 and 6, depending on the building specifications. This amount was in accordance with the examples found in (Contegni et al. 2008).

Figure 5.4: Structural configuration (Casotto et al. 2015) and assumed position of openings in a) Type 1 buildings and b) Type 2 buildings

Table 7: Classification of the building typologies used in this document

Class	Structural Configuration	Code Level	Design lateral load	Id code according to (Casotto et al. 2015)
1	Type 1	Pre-code	2%	T1-PC-2
2	Type 2	Pre-code	2%	T2-PC-2
3	Type 2	Low-code	7%	T2-LC-7

Table 8: Material properties randomly sampled for the simulated design of the building stock

Class	R_{ck} [MPa]	f_{sk} [MPa]
1, 2	35, 40, 45, 50	320, 380
3	45, 50, 55	380, 440

Table 9: Geometric dimensions randomly sampled for the generation of the building stock. μ and σ are the mean and standard deviation of the associated normal distribution

Class	Parameter	Distribution	μ	σ	min	max
1	L_{beam} [m]	Lognormal	2.7	0.3	8	30

	$L_{intercol}$ [m]	Lognormal	9	1	8	10
	H_{col} [m]	Lognormal	1.9	0.2	4	12
2, 3	L_{beam} [m]	Normal	8.7	2	8	10
	$L_{intercol}$ [m]	Normal	16.5	3.7	10	25
	H_{col} [m]	Normal	6.5	1.3	4	11

Table 10: Load cases randomly sampled as a function of the type of structures and the dimensions of the members. GR is the roof weight, GLB the lateral beam weight, GB the beam self-weight, Q1 and Q2 the accidental and snow weight, respectively

Load type		**Class 1**	**Class 2, 3**
GR [kN/m^2]	$L_{intercol}$ < 20 m	2.4	2.9
	$L_{intercol}$ > 20 m		1.6
GLB [kN/m]		2.4	
GB [kN/m]	L_{beam} < 16 m	3.6	4
	16 < L_{beam} < 22 m	5.2	6
	22 < L_{beam} < 24 m	6.85	7.5
	24 < L_{beam} < 28 m	7.5	8
	L_{beam} > 28 m	8.55	9.5
Q1 [kN/m2]	Normal distribution	μ = 2; σ = 0.4; min = 0.8; max = 3.2	
Q2 [kN/m2]	Normal distribution	μ = 2; σ = 0.4; min = 0.8; max = 3.2	

Table 11: Beam-to-column connection

Class	**Presence of a dowel**	**Capacity of a beam-to-column connection**
1,2	No	Friction force
3	Yes	Friction force+strength of the dowel

Table 12: Material properties randomly sampled to model the building stock

Class	**R_{ck} [MPa]**	**f_{sk} [MPa]**	
1, 2	35, 40, 45, 50	**Smooth**	**Ribbed**

	multiplied by γ_c	μ = 356 σ = 67.8	380 multiplied by γs
3	45, 50, 55 multiplied by γ_c	**Ribbed** 380 440, multiplied by γs	

Table 13: Over-strength factors used to model the building stock

Over-strength factor	μ	CoV
γ_s	1.15	7.5%
γc	1.3	15%

A.1.2 Numerical models

See Section 3.1.2.

A.2. MODELLING OF NON-STRUCTURAL COMPONENTS

Based on (Regione Toscana direzione generale politiche territoriali n.d.) the most common types of claddings in precast buildings in the Tuscany region are vertical precast panels, horizontal precast panels and concrete masonry infills. Here, all three types were considered for buildings in building class 1, whereas only vertical panels and masonry infills were taken into account for buildings in building classes 2 and 3, due to large spans between the portals. However, as discussed below, two different types of fastenings were considered in the case of horizontal panels, which means that altogether eight subclasses were defined (Table 14).

Table 14: Definition of considered subclasses of precast buildings

Subclass	Class	Non-structural components
1V	1	Vertical panels
1H-A		Horizontal panels (Fastening A)
1H-B		Horizontal panels (Fastening B)
1M		Masonry infills
2V	2	Vertical panels
2M		Masonry infills
3V	3	Vertical panels
3M		Masonry infills

A.1.1 Vertical and horizontal panels

Characteristics of vertical and horizontal panels

Vertical and horizontal panels were considered to be very stiff elements, attached, respectively, to the beams and columns (Isaković et al. 2012). The width of a single panel was limited to 2.5 m. The areal weight of the panels was estimated on the basis of the combined thickness of the concrete layers in the panels (Isaković et al. 2012), which was assumed to be a random variable.

At the bottom, vertical panels are most often restrained to the foundation beam, whereas horizontal panels are generally placed on vertical supports (i.e. steel corbels), implemented into columns (Isaković et al. 2012). The corbels prevent vertical and out-of-plane horizontal displacements, but allow in-plane horizontal drifts to some extent, due to a gap provided for the installation of the panels. These drifts lead to friction between the corbels and the panel. A uniform distribution with a wide interval of output values was assumed for the coefficient of friction, due to different materials being used in this connection. The characterization of parameters is summarised in Table 15.

At the top of both vertical and horizontal panels, fastenings are provided to prevent overturning. There are many different types of fastenings available on the Italian market, which can be divided into pinned and sliding ones, depending on their drift capacity. In the case of vertical panels, most commonly a sliding connection is used (denoted here as Fastening A), consisting of a hammer-head strap, which connects steel channels embedded in a panel and the supporting structural element (Isaković et al. 2012). In the case of horizontal panels, both sliding and pinned connections are commonly provided (Isaković et al. 2012). While the former are the same as in the case of vertical panels, the latter most frequently contain either a steel angle element or a steel box element. Since it was found that both types of pinned fastenings demonstrate similar behaviour, only the fastening containing steel box element (denoted here as Fastening B) is presented. The force-displacement relationships of fastenings are presented in Figure 5.5. Tensile out-of-plane capacity of fastenings was assessed according to information from different Italian producers. The parameters related to shear in-plane behaviour, on the other hand, were assessed according to cyclic tests, performed in the frame of the SAFECLADDING project (Isaković et al. 2013). Different hysteretic rules apply for each of the considered fastenings, as presented in Figure 5.5. Displacements and forces at the characteristic points of the force-displacement relationship (given in Table 16 and Table 17) were considered uniformly distributed. Large dispersion of these values is a consequence of the varying geometry, material properties, axial load and especially uncertainties associated with the installation of the fastenings. Correlation between characteristic points is not evident from the experimental results and was therefore not taken into account.

Openings were considered in a simplified manner. Their assumed location was presented in Figure 5.4. Doors were considered in one direction (frames in the X direction) by taking out two panels in one of the bays. In the other direction (frames in the Y direction) windows were considered by reducing the mass of the panels (Figure 3.5). The reduction factor was determined on the basis of the glazed area, which was treated as a random variable. The minimum and maximum fractions of the glazed area were assessed on the basis of the information from producers.

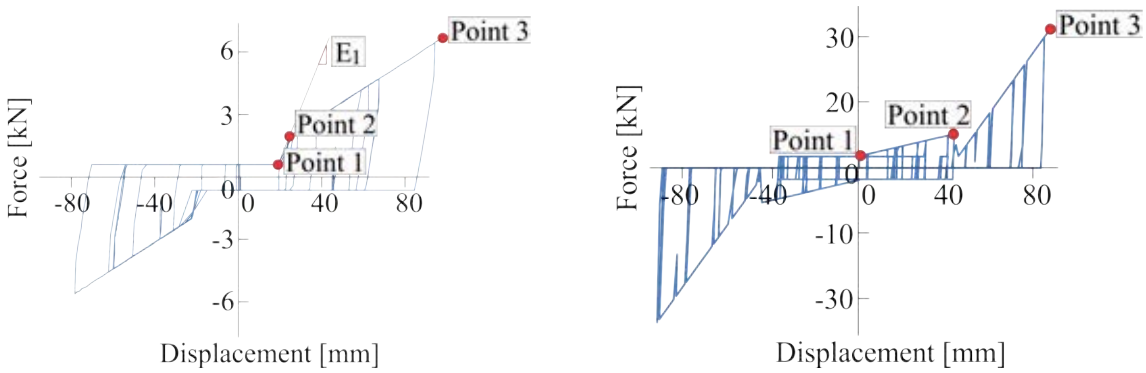

a) b)

Figure 5.5: a) force-displacement relationships, modelled in OpenSees (McKenna & Fenves 2010) a) of a shear fastening and b) of a pinned fastening

Table 15: Characteristics of vertical and horizontal panels

Parameter	Distribution	α^2	β^2	Source
Combined thickness of the concrete layers [cm]	Uniform	16	18	(Isaković et al. 2012)
Glazed area-vertical panels [%]	Uniform	7.5	20	Expert judgement, producers
Glazed area-bottom horizontal panels [%]	Uniform	50	90	Expert judgement, producers
Friction coefficient between corbels and horizontal panels [-]	Uniform	0.20	0.60	(Isaković et al. 2012)

Table 16: Characteristics of sliding fastenings

Parameter	Distribution	α^2	β^2	Source
In-plane Point 1 force [kN]	Constant	1	/	(Isaković et al. 2013)
In-plane Point 1 displacement [mm]	Uniform	19	36	(Isaković et al. 2013)
In-plane Point 2 force [kN]	Constant	3	/	(Isaković et al. 2013)
In-plane Young's modulus [kN/mm^2]	Constant	3	/	(Isaković et al. 2013)
In-plane Point 3 force [kN]	Uniform	5.1	9.7	(Isaković et al. 2013)

[2] Parameters of the distribution. In the case of uniform distribution, α and β are minimum and maximum, respectively. In the case of normal distribution, α and β are mean and standard deviation, respectively. In the case of constant distribution, α is the deterministic value.

In-plane Point 3 displacement [mm]	Uniform	50	100	(Isaković et al. 2013)
Out-of-plane Strength [kN]	Normal	27	1.35	Producers

Table 17: Characteristics of pinned fastenings

Parameter	Distribution	α[3]	β[2]	Source
In-plane Point 1 force [kN]	Uniform	4.5	5	(Isaković et al. 2013)
In-plane Point 2 force [kN]	Uniform	8.9	15.8	(Isaković et al. 2013)
In-plane Point 2 displacement [mm]	Uniform	35	40	(Isaković et al. 2013)
In-plane Point 3 force [kN]	Uniform	30	37	(Isaković et al. 2013)
In-plane Point 3 displacement [mm]	Uniform	50	56	(Isaković et al. 2013)
Out-of-plane Strength [kN]	Normal	25.5	1.28	Producers

Numerical models

See Section 3.1.3.1.

A.1.2 Masonry infills

Characteristics of masonry infills

Concrete masonry infills are usually situated between columns (Regione Toscana direzione generale politiche territoriali n.d.). A uniform distribution was assumed for the infill thickness, volumetric weight, shear modulus and shear strength with parameters assessed on the basis of a technical normative act (MIT 2009), a project report (Magrini et al. 2011) and information from construction company (Table 18). The considered infills have a poor connection with the adjacent beam, resulting in negligible vertical load being transmitted from the roof. If no out-of-plane restraints are provided as well, no arching mechanism is able to form and overturning of an infill can be prevented only by the self-weight of the infill and friction at the infill-to-column connection. Such failures were observed after recent Italian earthquakes (Belleri et al. 2014). The distribution of friction coefficient between infills and columns was assessed based on (Aslam et al. 1980).

In one direction (frames in the X direction) doors of a constant height and a varying length (following a uniform distribution) were considered. In the other direction (frames in the Y direction) windows reaching from column to column were considered in each bay. The window height was treated as a random variable with a uniform distribution.

[3] Parameters of the distribution. In the case of uniform distribution, α and β are minimum and maximum, respectively. In the case of normal distribution, α and β are mean and standard deviation, respectively. In the case of constant distribution, α is the deterministic value.

Table 18: Characteristics of masonry infills

Parameter	Distribution	Min	Max	Source
Thickness [cm]	Uniform	20	30	(Magrini et al. 2011)
Shear modulus [kN/m^2]	Uniform	600	880	(MIT 2009)
Shear strength [kN/m^2]	Uniform	18	24	(MIT 2009)
Volumetric Weight [kN/m^3]	Uniform	1360	1440	(MIT 2009), producers
Friction coefficient between infills and columns [-]	Uniform	0.18	0.60	(Aslam et al. 1980)
Window height [m]	Uniform	1	2	Expert judgement
Door length [m]	Uniform	2	4	Expert judgement

Numerical models of masonry infills

See Section 3.1.3.2.

A.3. DEFINITION OF DAMAGE STATES

A.3.1. Structure damage states

See Section 3.1.4.1.

A.3.2. Damage states of non-structural elements

See Section 3.1.4.2

A.4. SEISMIC INPUT FOR REGIONAL FRAGILITY FUNCTIONS

The ground motion records used in the fragility analysis were the same as those used in (Casotto et al. 2015). Fifty-seven seismic events (each consisting of three recorded ground motions; one for each direction) have been selected from the PEER database (PEER 2013). For thirteen of them, additionally, a scale factor of up to 1.5 was used, which altogether amounted to 70 dynamic analyses per building. The record set in (Casotto et al. 2015) was chosen to match magnitude M_w and distance R, which contributed most to the 475 years return period hazard and 2475 years return period hazard for spectral acceleration at 1.5 s in Northern Italy. These values obtained by (Iervolino et al. 2011) are given in Table 19. Furthermore, soil profile was also considered. The soil in this area is classified as soft according to classification from Eurocode 8 (CEN 2004b).

Table 19: Target magnitude M_w and distance R used in ground motion selection (Iervolino et al. 2011)

Hazard (S_a(1.5s))	Magnitude M_w	Distance R
475 years return period	4-6.5	0-20km
2475 years return period	4.5-6.5	0-30km

A.5. METHOD FOR GENERATION OF FRAGILITY FUNCTIONS

The methodology described in Section 3.1.1 allows the intensity measure to be selected after the dynamic analyses are performed. This feature was exploited by (Casotto et al. 2015), who made an effort of finding the so-called optimal period at which the geometric mean of spectral acceleration yielded the best match between numerical results and corresponding fragility function. However, in order to be more consistent with the fragility functions for contents, which have been obtained from literature (see Section 3.2), in this illustrative example the geometric mean of PGA was chosen for the intensity measure. Note that the intensity measure can be replaced with little computational effort once the dynamic analyses are performed.

Each subclass is represented by 100 buildings and altogether 800 were generated. For each of the 800 buildings a three dimensional numerical model was built. For each model 70 non-linear dynamic analyses were then performed using the set of ground motions described in Section A.4.

All the analyses were performed in Opensees (McKenna & Fenves 2010). Mass and initial stiffness proportional damping was assumed with the 2% ratio of critical damping. The same ratio was used by (Casotto et al. 2015), who, on the other hand, assumed tangent stiffness proportional damping. The P-Δ effect was taken into account. During the analyses collapse criteria for non-structural elements were also checked. If any of the criteria for any non-structural element was met, that non-structural element was considered dislocated from the structure and was removed from the model immediately during the analysis. Similarly, during the analyses of buildings in building class 3, performance of the dowel connections was checked. If the strength of a certain dowel was attained, the dowel was removed from the model during the analysis.

The results of dynamic analyses were then used to form a damage probability matrix, which presents, for each seismic event and corresponding intensity, a ratio of buildings per subclass that reached a certain damage state. Fragility curves were then formed using regression analysis on the cumulative percentage of buildings in each damage state for a set of intensity levels. A lognormal distribution was assumed. The regression analysis was carried out using the maximum likelihood method as proposed by (Baker 2014b) and (Baker 2014a).

A.6. FINAL FRAGILITY FUNCTIONS

In this section, fragility functions for all subclasses are presented. DS4 fragility functions (dislocation of at least 30% of non-structural elements) for all considered subclasses are presented along with the corresponding results from dynamic analyses. All fragility functions for non-structural and structural components of all considered subclasses are presented. Fragility functions for non-structural components are indicated as DS1, DS2, …, DS11,

which corresponds to damage states as defined in Section 3.1.4.2. Fragility functions for structural components are indicated as moderate, extensive, near complete and complete, which, again, corresponds to damage states as defined in Section 3.1.4.1. Consequences of designated damage states or so-called damage-loss models are presented in Section 4.1.

Subclass 1V (Class 1 + Vertical panels)

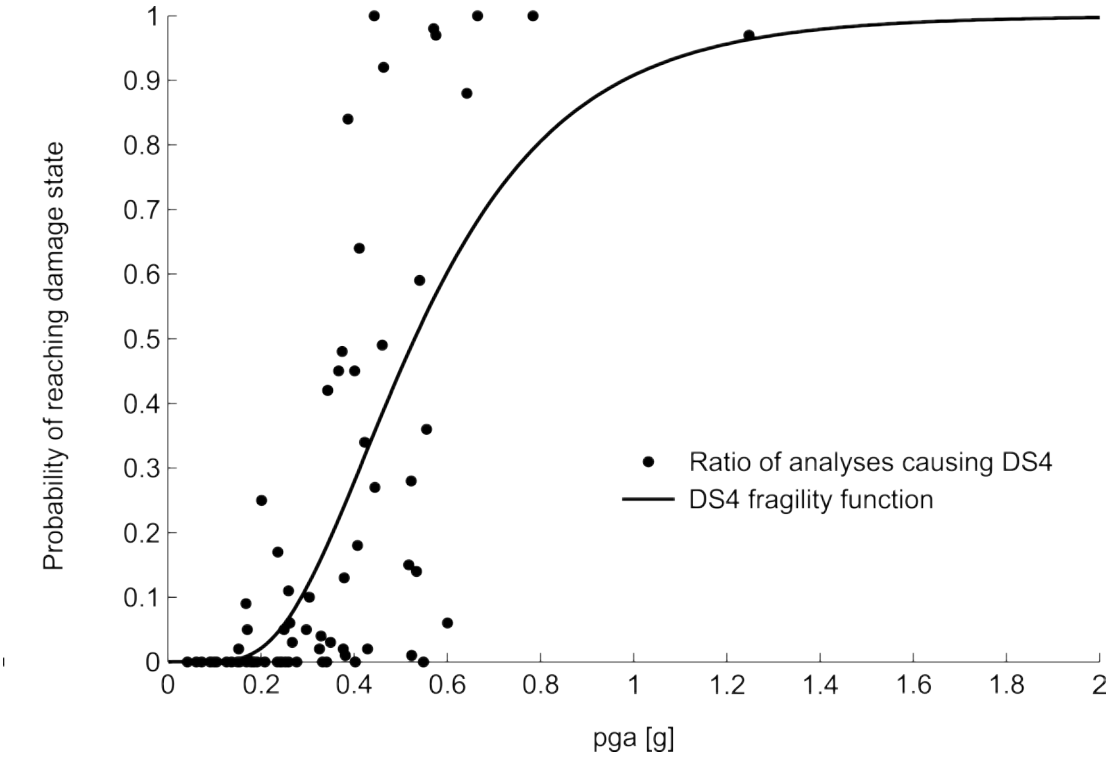

Figure 5.6: DS4 (At least 30% of vertical panels dislocated) fragility function with results from dynamic analyses for subclass 1V

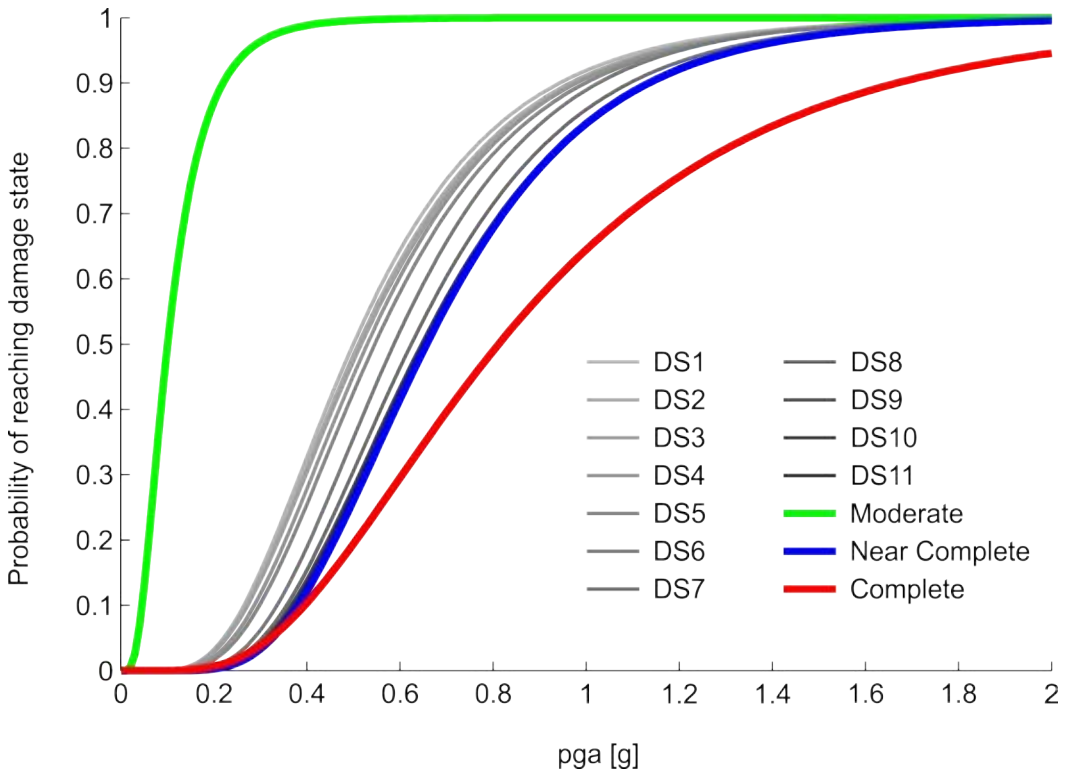

Figure 5.7: Structural and non-structural fragility functions for subclass 1V

Subclass 1H-A (Class 1 + Horizontal panels (Fastening A))

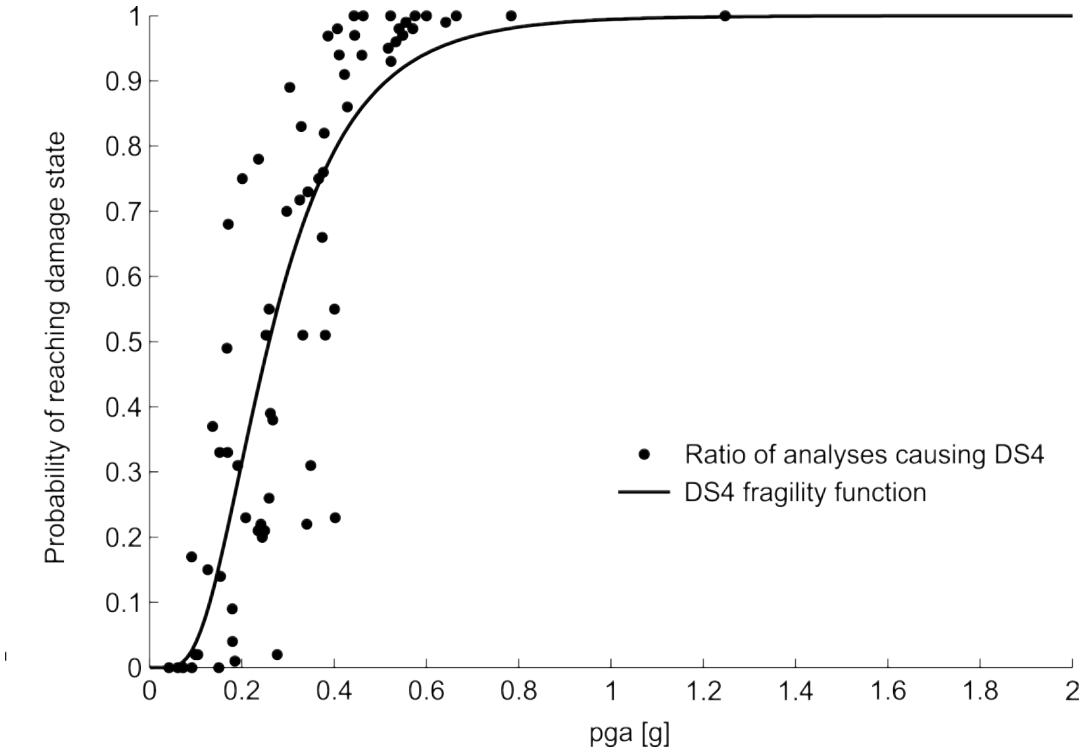

Figure 5.8: DS4 (At least 30% of horizontal panels dislocated) fragility function with results from dynamic analyses for subclass 1H-A

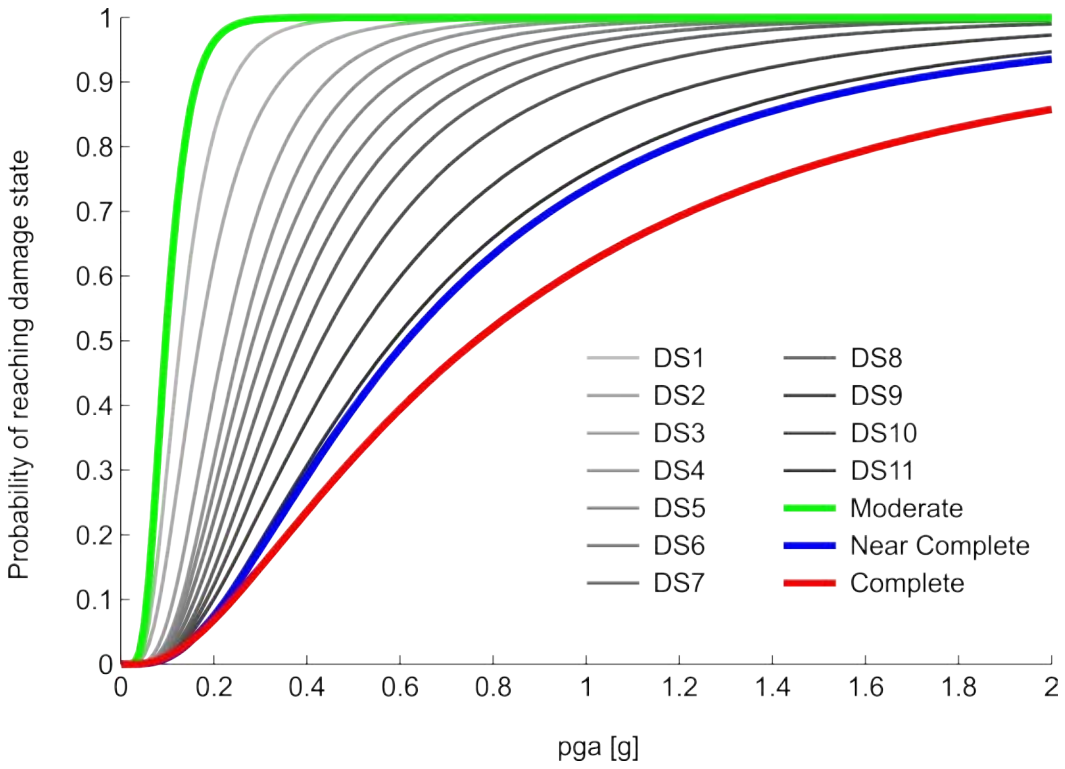

Figure 5.9: Structural and non-structural fragility functions for subclass 1H-A

Subclass 1H-B (Class 1 + Horizontal panels (Fastening B))

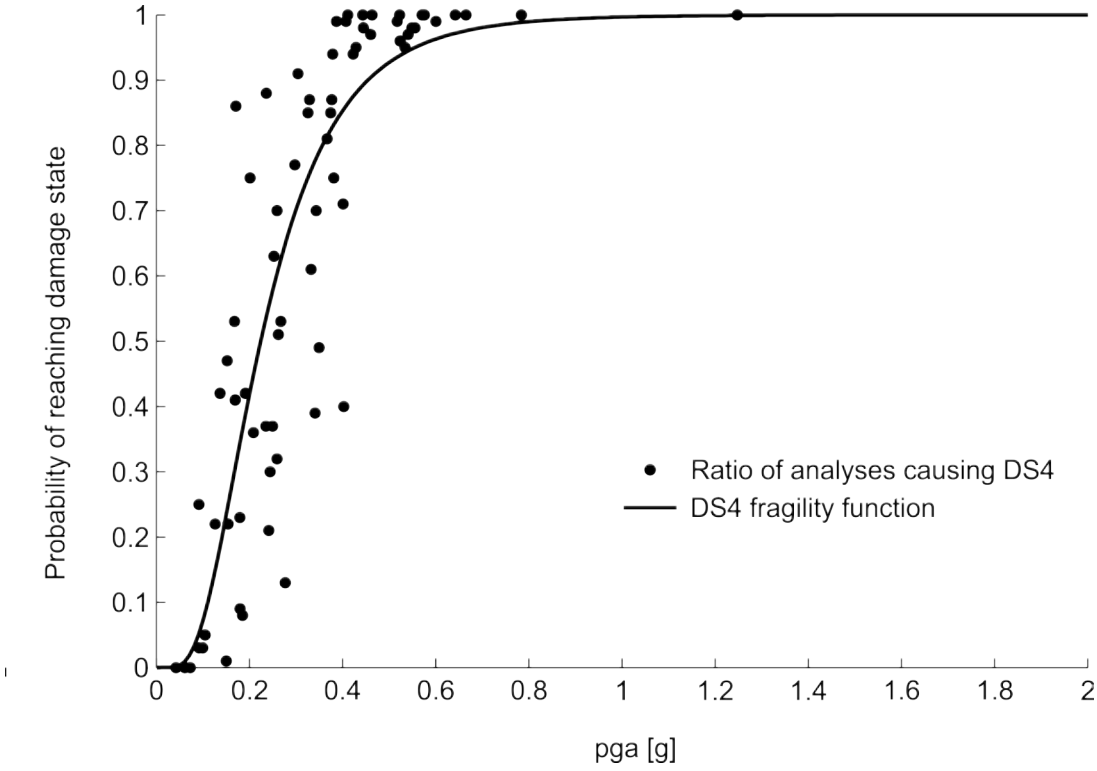

Figure 5.10: DS4 (At least 30% of horizontal panels dislocated) fragility function with results from dynamic analyses for subclass 1H-B

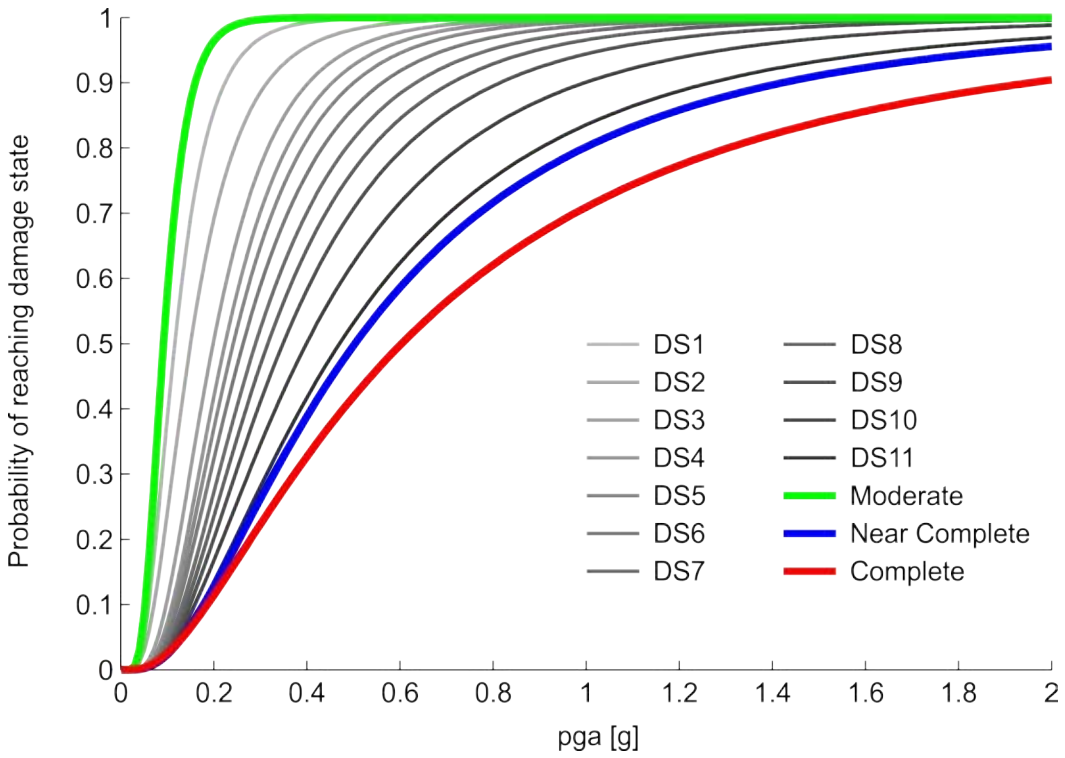

Figure 5.11: Structural and non-structural fragility functions for subclass 1H-B

Subclass 1M (Class 1 + Masonry infills)

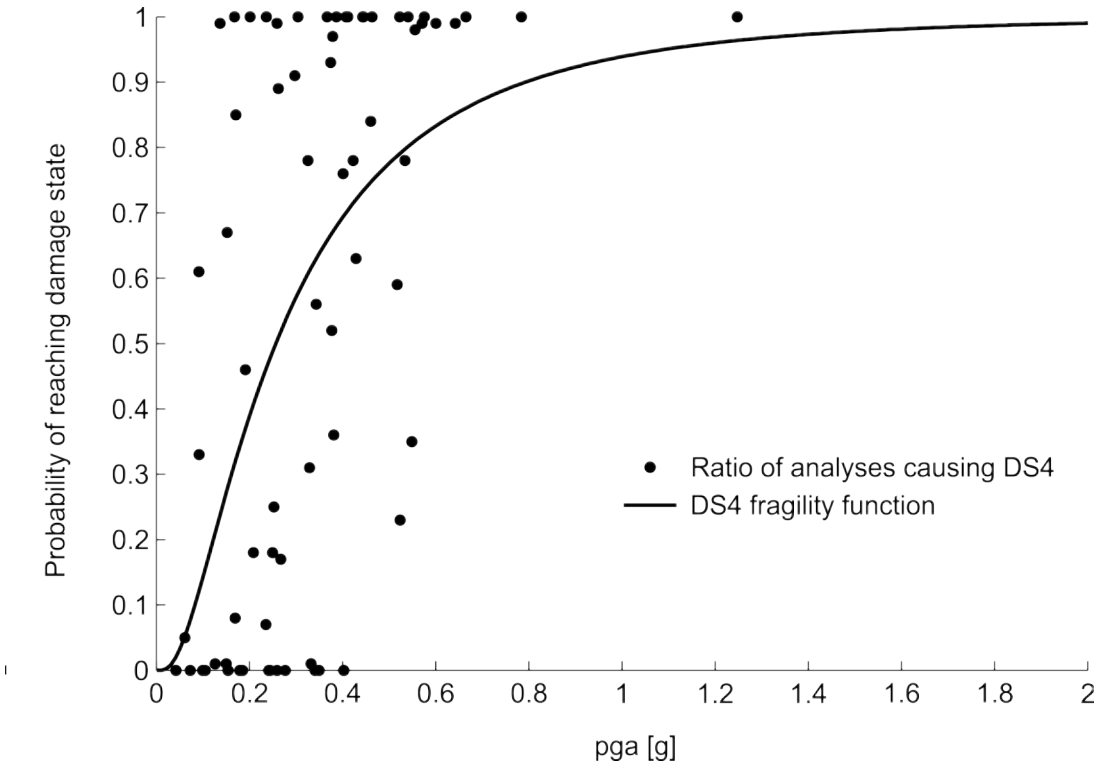

Figure 5.12: DS4 (At least 30% of masonry infills dislocated) fragility function with results from dynamic analyses for subclass 1M

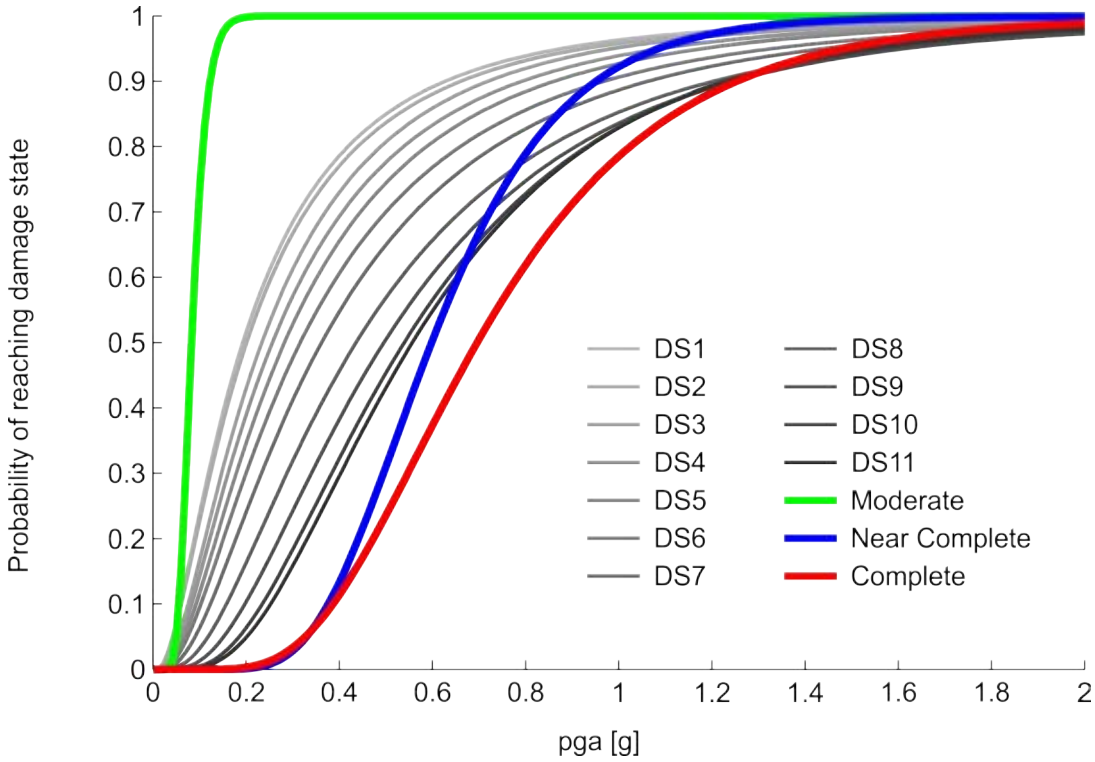

Figure 5.13: Structural and non-structural fragility functions for subclass 1M

Subclass 2V (Class 2 + Vertical panels)

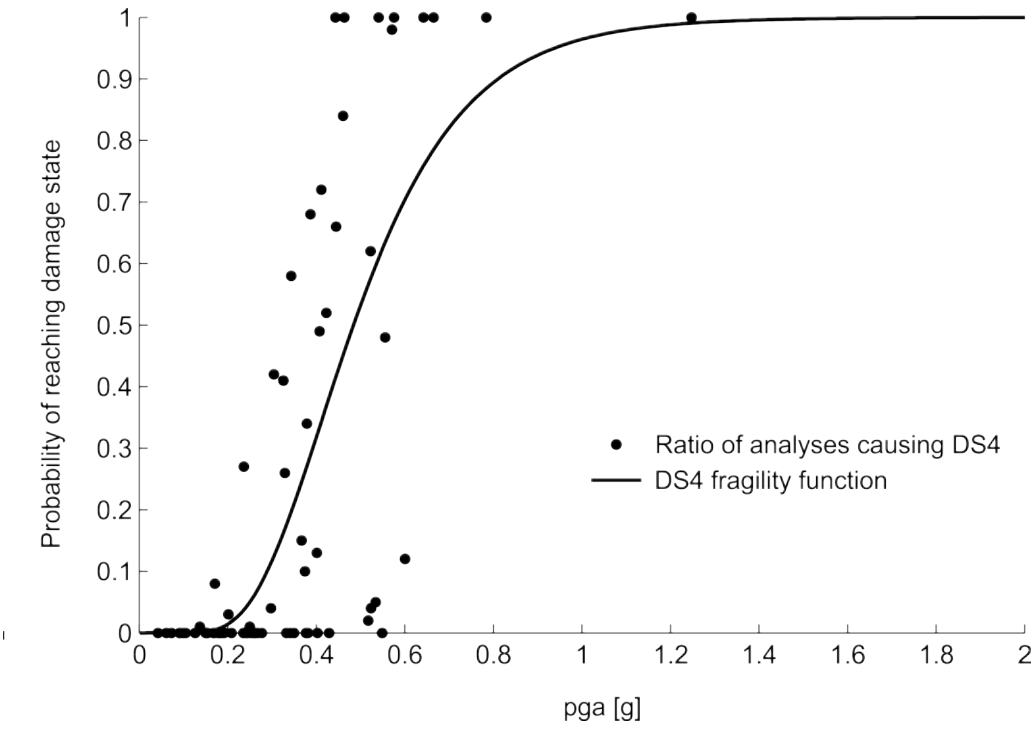

Figure 5.14: DS4 (At least 30% of vertical panels dislocated) fragility function with results from dynamic analyses for subclass 2V

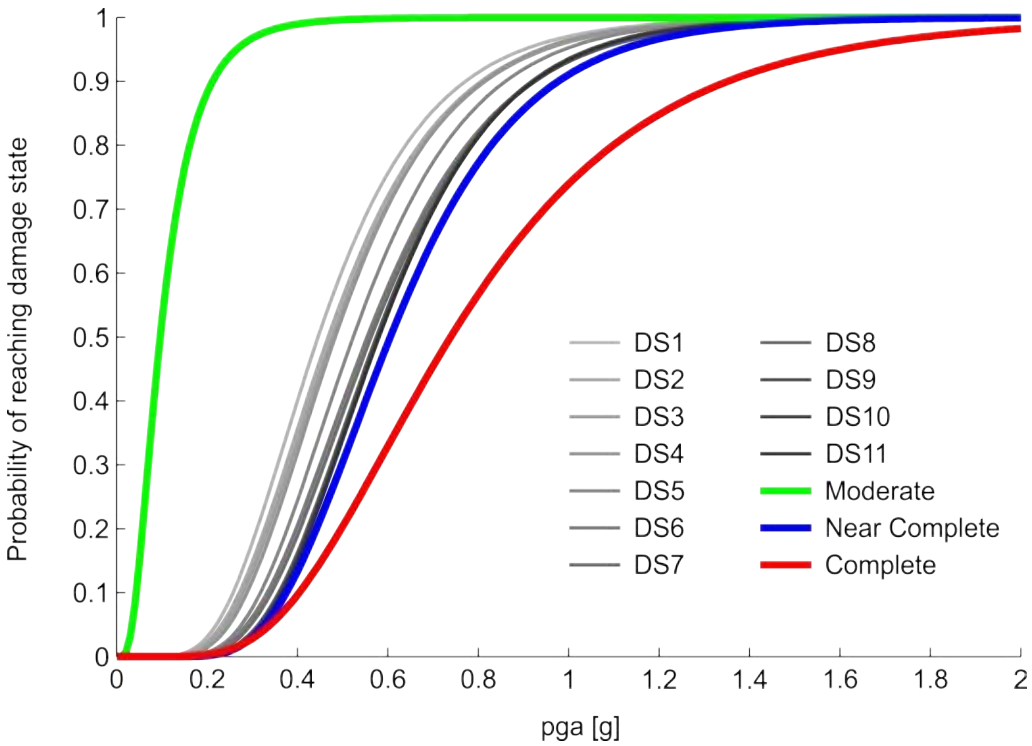

Figure 5.15: Structural and non-structural fragility functions for subclass 2V

Subclass 2M (Class 2 + Masonry infills)

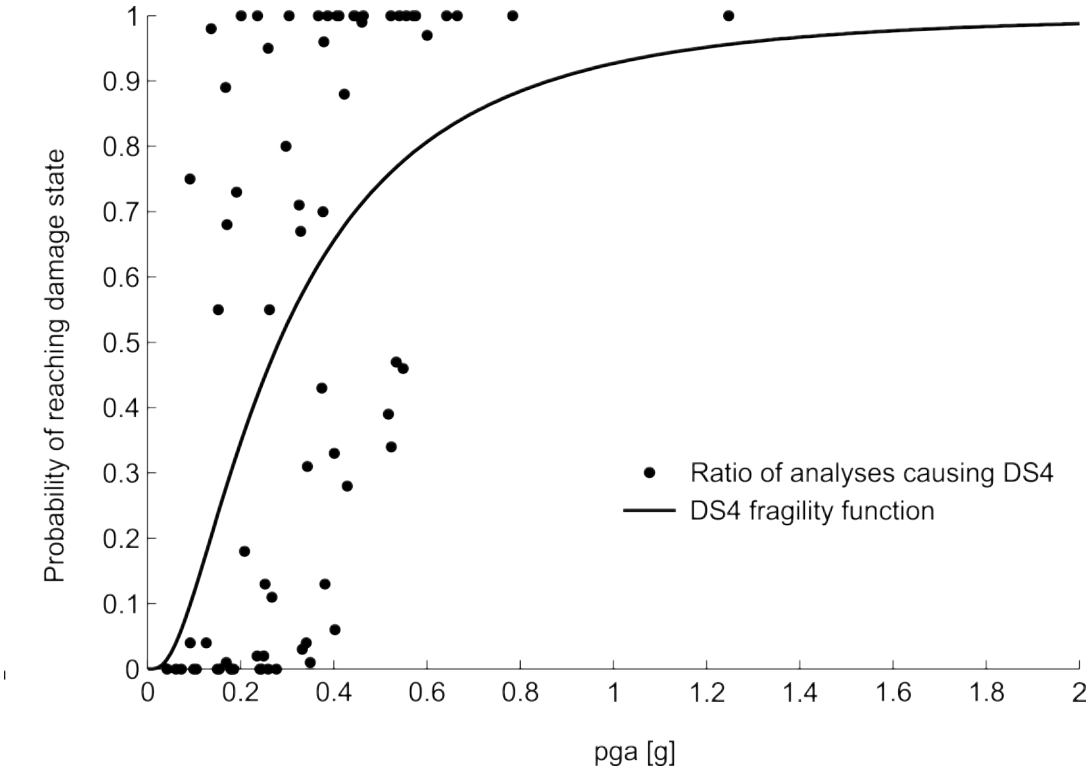

Figure 5.16: DS4 (At least 30% of masonry infills dislocated) fragility function with results from dynamic analyses for subclass 2M

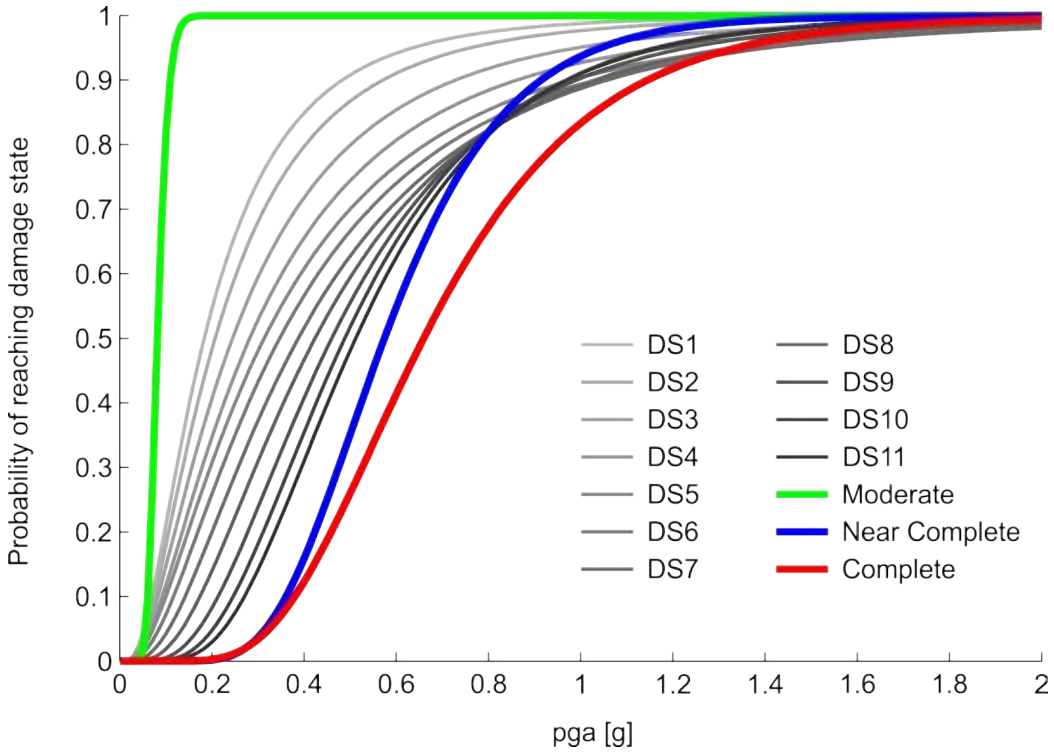

Figure 5.17: Structural and non-structural fragility functions for subclass 2M

Subclass 3V (Class 3 + Vertical panels)

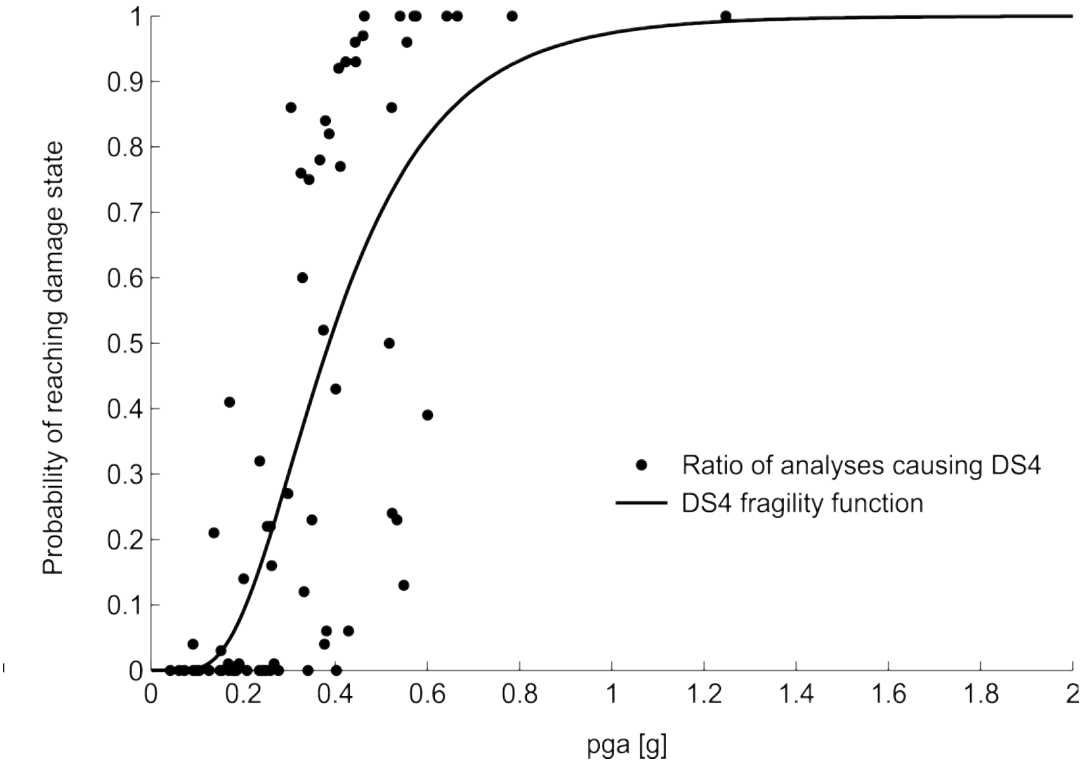

Figure 5.18: DS4 (At least 30% of vertical panels dislocated) fragility function with results from dynamic analyses for subclass 3V

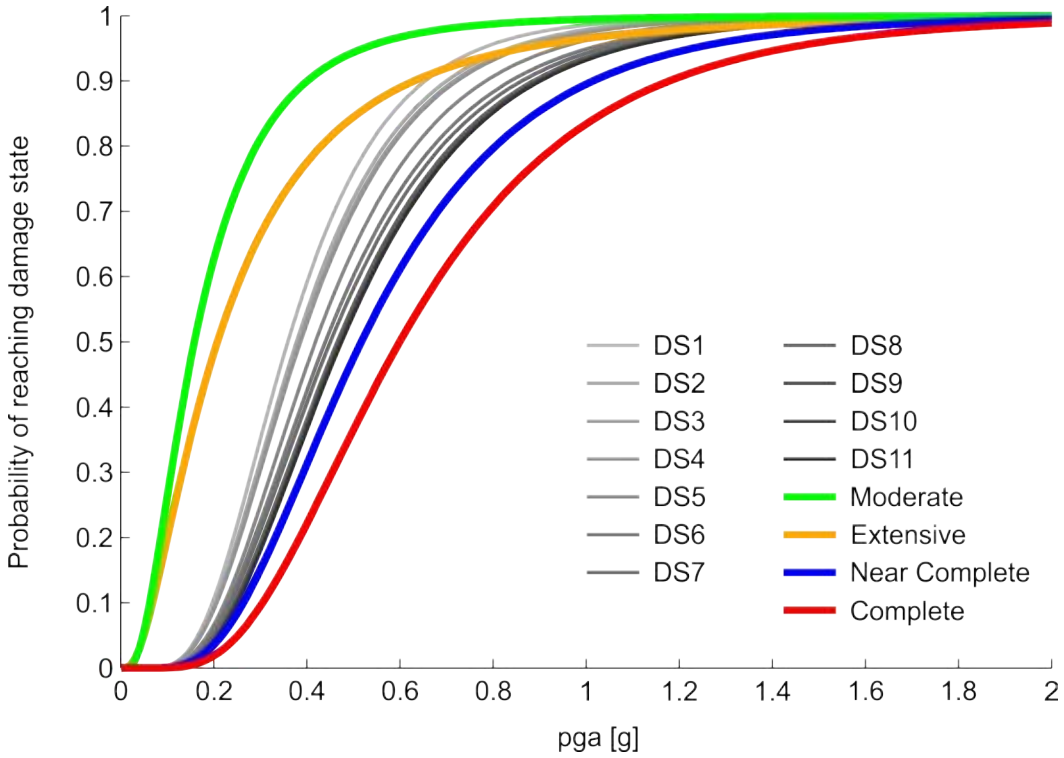

Figure 5.19: Structural and non-structural fragility functions for subclass 3V

Subclass 3M (Class 3 + Masonry infills)

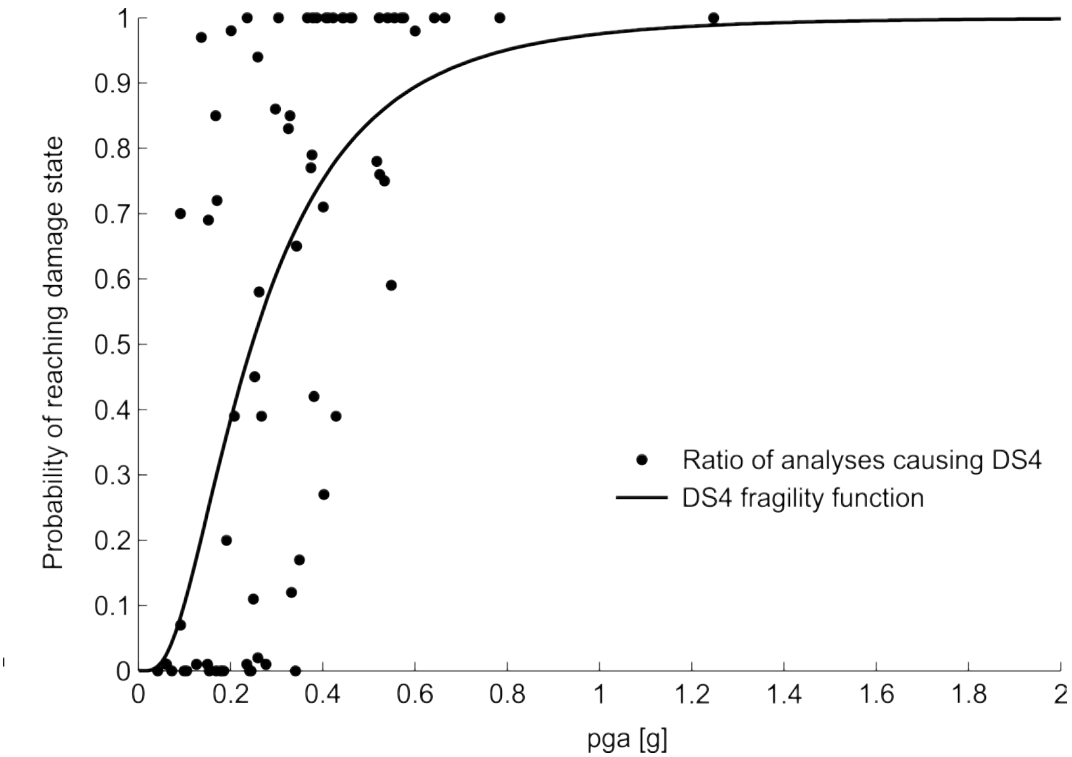

Figure 5.20: DS4 (At least 30% of masonry infills dislocated) fragility function with results from dynamic analyses for subclass 3M

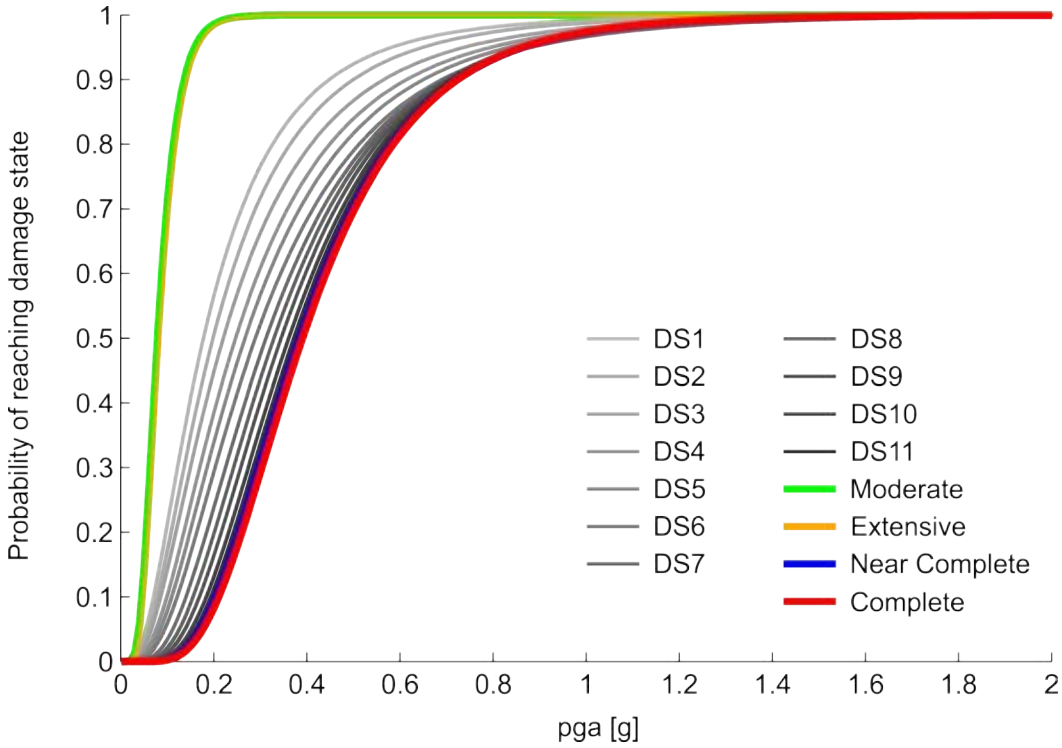

Figure 5.21: Structural and non-structural fragility functions for subclass 3M

A.7. COMMENTARY

Non-structural components affect structural performance in different aspects. Firstly, increased stiffness and mass most often decrease the period of the structure, which is, in this case, detrimental due to the enlargement of spectral acceleration. Secondly, large masses of the non-structural components represent additional inertial forces. And thirdly, if non-structural components are attached to the columns, the gain in stiffness leads to smaller deformations at the bases of the columns, but larger shear forces in the beam-to-column connections. In other words, as stiffness increases, beam-to-column connections become more at risk. On the other hand, if non-structural components are attached to the beams, as in the case of vertical panels, the increase in stiffness is beneficial since it decreases the displacements of the roof and consequently the demand on the beam-to-column connections. For these reasons, horizontal panels have the most detrimental effect on the structural performance. Not only their entire mass is translated into the structure, but their attachment to the columns increases demand on the beam-to-column connection. This phenomenon is more severe in the case of buildings with pinned panel-to-column connections (subclass 1H-B) comparing to buildings with sliding panel-to-column connections (subclass 1H-A), which is why the former are more fragile than the latter. In order to be conservative, it is therefore advised that pinned connections are assumed, if no additional information is available. Similarly to horizontal panels, masonry infills increase the stiffness of the portals by being attached to the columns, which leads to higher demand in beam-to-column connections. Additionally, in some cases collapse occurs due to continuous windows at the top, resulting in the effect of short columns. Oppositely, the attachment of vertical panels to the beams increases the stiffness in a favourable manner, since it reduces demand on the beam-to-column connection. Moreover, in contrast to horizontal panels only one half of their mass is translated into the structure; the other one being transferred directly

to the foundation. According to these findings, it is necessary to account for the presence of the panels or the infills, if one wants to realistically assess the structural performance, which is in accordance with comments made by (Bournas et al. 2013) and (Colombo et al. 2014).

Furthermore, the comparison of fragility parameters of classes V2 and V3 given in Table 21 indicates that buildings with higher design level are more fragile. This is at first glance surprising, if not paradoxical. However, higher design level reflects in stiffer buildings, which results in higher seismic demand. Furthermore, the implementation of dowels, combined with an impropriate design of the corbels, which they are inserted in, may have a detrimental effect. If a dowel connection fails globally (i.e., by the spalling of surrounding concrete), it has practically no ductility, which, in combination with low strength (i.e., ranging from 40kN to 96kN), means that it often performs worse than a friction-only connection, due to its lower sliding capacity. This is even more crucial in buildings with masonry infills, where beam-to-column connections are exposed to greater demand, as discussed above. Median collapse (complete damage state) PGA for subclass 2M equals 0.66g, whereas median collapse PGA for subclass 3M amounts only to 0.39g. This does not imply, of course, that we should design buildings with friction-only connections, but merely that dowel connections should be appropriately designed in order to provide sufficient strength and ductility.

It should be noted that results based on the fitted fragility functions may not be realistic in some cases due to statistical methods used for assessing the fragility parameters. For example, in the case of the fragility functions for type 1 buildings with horizontal panels (subclass 2) it can be observed that the probability of occurrence of major damage is greater in comparison to the probability of occurrence of minor damage. Such a problem can be expected in the case of damage states being close to one another, e.g., when looking at damage states corresponding to 70% of infills dislocated and 80% of infills dislocated. In general, overlapping of fragility functions will appear in the case of different logarithmic standard deviations, but in regions, which are not important for engineers, i.e., when fragility functions take values very close to 0 or 1. In this case, however, overlapping begins in regions of fragility functions closer to the medians of fragility functions. It is therefore advised to take the envelope of fragility functions if overlapping occurs. This implies that damage states are dependent, which a reasonable assumption is considering the damage state definition, i.e., damage is accumulating with each higher damage state.

Table 20: Parameters (median θ and logarithmic standard deviation β) of fragility functions for non-structural components

Subclass	DS1		DS2		DS3		DS4		DS5		DS6		DS7		DS8		DS9		DS10		DS11	
	θ [g]	β	θ [g]	β	θ [g]	β	θ [g]	β	θ [g]	β	θ [g]	β	θ [g]	β	θ [g]	β	θ [g]	β	θ [g]	β	θ [g]	β
V1	0.50	0.50	0.51	0.50	0.52	0.50	0.53	0.48	0.55	0.47	0.59	0.44	0.62	0.44	0.65	0.44	0.65	0.44	0.65	0.44	0.65	0.44
H1-p	0.12	0.51	0.15	0.58	0.20	0.55	0.22	0.55	0.24	0.57	0.26	0.59	0.29	0.61	0.32	0.63	0.35	0.66	0.40	0.71	0.47	0.77
H1-s	0.13	0.49	0.17	0.55	0.22	0.53	0.26	0.53	0.28	0.57	0.31	0.59	0.35	0.61	0.39	0.62	0.43	0.66	0.50	0.72	0.59	0.76
M1	0.19	0.92	0.20	0.93	0.23	0.88	0.26	0.88	0.28	0.87	0.32	0.87	0.36	0.84	0.44	0.79	0.50	0.72	0.54	0.65	0.56	0.62
V2	0.45	0.43	0.47	0.42	0.48	0.42	0.48	0.40	0.52	0.39	0.55	0.40	0.56	0.39	0.58	0.37	0.58	0.36	0.58	0.36	0.58	0.36
M2	0.18	0.75	0.21	0.79	0.25	0.85	0.28	0.87	0.31	0.89	0.35	0.85	0.39	0.78	0.42	0.69	0.46	0.60	0.49	0.53	0.51	0.50
V3	0.36	0.47	0.38	0.48	0.38	0.49	0.39	0.49	0.42	0.49	0.44	0.50	0.45	00.51	0.47	0.50	0.47	0.50	0.47	0.50	0.47	0.50
M3	0.18	0.72	0.20	0.72	0.22	0.73	0.25	0.71	0.27	0.69	0.29	0.68	0.31	0.62	0.33	0.59	0.34	0.56	0.36	0.53	0.37	0.51

Table 21: Parameters (median θ and logarithmic standard deviation β) of fragility functions for structural components

Subclass	Moderate		Extensive		Near complete		Complete	
	θ [g]	β	θ [g]	β	θ [g]	β	θ [g]	β
V1	0.10	0.61	/	/	0.66	0.43	0.81	0.56
H1-p	0.09	0.43	/	/	0.50	0.81	0.60	0.92
H1-s	0.10	0.41	/	/	0.61	0.78	0.76	0.90
M1	0.08	0.30	/	/	0.60	0.36	0.70	0.46
V2	0.10	0.61	/	/	0.61	0.37	0.74	0.47
M2	0.08	0.23	/	/	0.57	0.36	0.66	0.43
V3	0.16	0.72	0.21	0.87	0.52	0.53	0.60	0.53
M3	0.08	0.43	0.08	0.43	0.39	0.49	0.39	0.48